

X-RAY COMPUTED TOMOGRAPHY FOR PERFORMING POLYMER GEL
DOSIMETRY: A FEASIBILITY STUDY

by

MICHELLE LOUISE HILTS

B.Sc., McMaster University, 1996

B.A., McMaster University, 1996

A THESIS SUBMITTED IN PARTIAL FULFILMENT OF
THE REQUIREMENTS FOR THE DEGREE OF

MASTER OF SCIENCE

in

THE FACULTY OF GRADUATE STUDIES

(Department of Physics and Astronomy)

We accept this thesis as conforming
to the required standard

THE UNIVERSITY OF BRITISH COLUMBIA

September 1999

© Michelle Louise Hiltz, 1999

In presenting this thesis in partial fulfilment of the requirements for an advanced degree at the University of British Columbia, I agree that the Library shall make it freely available for reference and study. I further agree that permission for extensive copying of this thesis for scholarly purposes may be granted by the head of my department or by his or her representatives. It is understood that copying or publication of this thesis for financial gain shall not be allowed without my written permission.

Department of Physics and Astronomy

The University of British Columbia
Vancouver, Canada

Date 13 Oct. 1999

ABSTRACT

Radiation therapy treatment of cancer is increasingly concerned with delivering dose distributions that conform to the tumour volume. For verification of treatment planning computer dose calculations, these conformal therapies demand an accurate, sensitive, high resolution three dimensional (3D) dosimeter. Polymer gels are novel, inherently 3D, tissue equivalent radiation dosimeters. Traditionally, dose distributions recorded in polymer gel are read out using magnetic resonance imaging (MRI). Presented here is a feasibility study on a new 3D dosimetry technique that uses x-ray computed tomography (CT) to read dosimetric information from polymer gels. The technique exploits a gel density change that occurs in response to ionizing radiation. This study has three main goals: 1) to develop a protocol for producing quality CT polymer gel images; 2) to evaluate the nature and reproducibility of the dosimeter's CT number (N_{CT})-dose response; and 3) to compare this technique with MRI polymer gel dosimetry. A quantitative discussion of the density changes occurring in the gel in response to ionization radiation is also provided. Experiments are conducted using a PAG (polyacrylamide and gelatin) gel dosimeter irradiated with four intersecting 10 MV photon beams. The N_{CT} -dose response is found to be linear and reproducible over the range of 200 to 1000cGy. At room temperature the response is $(8.7 \pm 0.3) \times 10^{-3} N_{CT}/\text{cGy}$ resulting in a limited dose resolution, ~ 100 cGy. Gel temperature during imaging is determined to have only a small effect, $0.3\%/^{\circ}\text{C}$, on the dose response. Spatial resolution is 0.5 mm in the image plane and 10mm-1mm (depending on noise requirements) in the third dimension. Despite the low dose resolution, preliminary results indicate this technique provides accurate localization of high dose regions and, given the availability and speed of CT imaging, has the potential to be a valuable and practical tool for radiation therapy clinics.

TABLE OF CONTENTS

Abstract	ii
List of Tables	v
List of Figures	vi
Acknowledgments	ix
CHAPTER 1 Introduction	3
1.1 Motivation for a 3D Dosimeter	3
1.2 Standard Dosimeters and Dose Measurement in 3D	4
1.3 A Brief History of Gel Dosimetry	7
1.4 Motivation for X-ray Computed Tomography Gel Dosimetry	10
CHAPTER 2 Background Information	13
2.1 Radiation Dosimetry Theory	13
2.1.1 Radiation Absorbed Dose	13
2.1.2 Clinical Dosimetry	18
2.1.3 Relative and Absolute Dosimetry	19
2.2 PAG gel and Radiation Reactions	21
2.2.1 Water Radiolysis	22
2.2.2 Radical Chain Polymerization	22
2.2.3 Polymerization and Crosslinking in PAG gel	24
2.3 X-ray Computed Tomography	26
2.3.1 Conventional Imaging with X-rays	27
2.3.2 The Basics of X-ray Computed Tomography	28
2.3.3 CT Numbers	30
2.3.4 Density and CT Number	31
2.3.5 Noise and Physical Limitations	32

CHAPTER 3	Materials and Methods	35
3.1	General Gel Dosimetry Technique	35
3.2	Gel Preparation and Irradiation	36
3.3	CT Imaging Technique	38
3.4	Image Processing	40
3.5	Dose Measurements	41
3.6	Techniques for Determining PAG Gel Density	42
CHAPTER 4	Results and Discussion	46
4.1	CT Imaging Protocol	47
4.1.1	Optimum CT Imaging Parameters	48
4.1.2	Signal to Noise Ratio and Image Averaging	55
4.1.3	Artifacts	59
4.1.4	Digital Image Filtering	62
4.1.5	Summary of CT Imaging Protocol	64
4.2	CT Number – Dose Response	65
4.2.1	Characterization of the N_{CT} – Dose Response	65
4.2.2	Reproducibility of the N_{CT} – Dose Response	67
4.2.3	Effect of PAG Gel Imaging Temperature	73
4.3	Comparison of CT and MRI Techniques	76
4.3.1	Dose Measurement and Localization of High Dose Regions	77
4.3.2	Dosimeter Characteristics: Advantages and Disadvantages	78
4.4	Quantifying PAG Gel Density	81
4.4.1	Density of Non-irradiated PAG Gel	81
4.4.2	Density Change for a High Dose	82
CHAPTER 5	Conclusions and Summary	84
References	89
Appendix I	94

LIST OF TABLES

	Page
Table 3.1	40
Parameter settings used for PAG gel CT imaging experiments on the GE HiSpeed CT/i [®] CT scanner.	
Table 4.1	64
Optimum parameter settings for imaging PAG gels with a GE HiSpeed CT/i [®] CT scanner.	
Table 4.2	78
Dosimeter characteristics measured for CT PAG gel dosimetry using a GE HiSpeed CT/i [®] CT scanner and the optimum imaging protocol described in section 4.1. For comparison, MRI PAG gel dosimetry characteristics are cited from literature (Olsson, 1998, Audet, 1997, Ibbott, 1997 and Maryanski, 1994).	

LIST OF FIGURES

	Page
Figure 1.1	3
An illustration of dose sparing as a result of conformal radiotherapy. Figures 1.1a and 1.1b show examples of the type of high dose region (represented in black) resulting from, respectively, a typical four field treatment and a multi-leaf collimator conformal treatment. Greater sparing of healthy tissue from high doses is evident with the conformal treatment. The cross - hatched area represents the clinical target volume (ICRU 50, 1993).	
Figure 2.1	15
Schematic illustration of the three interactions of photons with matter that are important for dose deposition in tissue.	
Figure 2.2	25
The chemical composition of acrylamide, N, N'-methylenebisacrylamide (Bis) and cross-linked polyacrylamide.	
Figure 3.1	36
A general overview of the gel dosimetry technique.	
Figure 3.2	37
Set-up of the cylindrical PAG gel dosimeter for irradiation with a medical linear accelerator (LINAC).	
Figure 3.3	38
Top view schematic of the cylindrical PAG gel used in this investigation. The arrangement of the four intersecting 3x3cm ² beams used in irradiation is illustrated. The depth of maximum dose (d_{max}) for 10MV photon beams, ~ 2.5 cm, is illustrated by black dots.	
Figure 3.4	39
Schematic diagram illustrating the orientation of the PAG gel CT images perpendicular to the cylindrical axis of the gel.	
Figure 3.5	45
The relationship between measured N_{CT} and the known density of various materials for the GE HiSpeed CT/i [®] CT scanner. All CT measurements were performed during a single scan with a tube voltage setting of 120 kV.	
Figure 4.1	46
Preliminary CT scan across a PAG Gel irradiated, as described in section 3.3, with four intersecting beams (2,4,6 and 8Gy at d_{max}). Beneath the high noise the expected star pattern result is just visible in this image.	

Figure 4.2	50
Sensitivity of N_{CT} to various densities near the density of water for all the tube voltage (kV) setting available on the GE HiSpeed $CT/i^{\text{®}}$ CT scanner.	
Figure 4.3	53
Image noise is reduced in CT images by increasing the operating tube current.	
Figure 4.4	56
Intensity profiles indicating the reduction of image noise with image averaging.	
Figure 4.5	58
Increase in SNR obtained from N averaged images of the PAG gel compared with the \sqrt{N} increase expected from theory. SNR measurements are also compared for images with slice thicknesses of 10 and 5 mm.	
Figure 4.6	60
Noise reduced PAG gel CT image showing ring and beam hardening artifacts that obscure dose information. This image was produced using optimum imaging parameters and averaging 64 images.	
Figure 4.7	61
Final processed PAG gel CT image showing clearly the star pattern dose distribution resulting from a four field irradiation.	
Figure 4.8	63
Effect of digital filtering a PAG gel CT image using a 3x3 median filter. Noise is reduced without compromising accurate localization of the high dose region.	
Figure 4.9	66
The N_{CT} – dose response of a PAG gel dosimeter. The dosimeter temperature was 23°C and the CT imaging protocol was employed (refer to section 4.1.5). N_{CT} increases linearly with dose up to a point and then increases more slowly as higher doses are reached. Error bars represent the standard deviation in the average dose measured in regions of interest. Error in N_{CT} , not illustrated, is +/- 0.5 H for all data points.	
Figure 4.10	68
The PAG gel's N_{CT} – dose response for images obtained with the gel at different positions in the CT scanner. For all images the CT imaging protocol was employed (refer to section 4.1.5). Error bars represent the standard deviation in the average dose measured in regions of interest. Error in N_{CT} , not illustrated, is $\pm 0.5 N_{CT}$ for all data points.	

Figure 4.11	69
<i>N_{CT}</i> - response curves obtained for the PAG gel dosimeter during a single imaging session. The dosimeter temperature was 23°C and the CT imaging protocol was employed (refer to section 4.1.5). Error bars represent the standard deviation in the average dose measured in regions of interest. The error in <i>N_{CT}</i> is only $\pm 0.5 N_{CT}$ for all data points and therefore is not illustrated.	
Figure 4.12	71
Shift in image intensity or grayscale measured over time into the imaging session for different regions in the PAG gel.	
Figure 4.13	72
<i>N_{CT}</i> - dose response curves obtained for the four field PAG gel dosimeter over a series of several imaging sessions. The dosimeter was at 23°C and the CT imaging protocol was employed (refer to section 4.1.5). Error bars represent the standard deviation in the average dose measured in regions of interest. Error in <i>N_{CT}</i> , not illustrated, is $\pm 0.5 N_{CT}$ for all data points.	
Figure 4.14	74
<i>N_{CT}</i> - dose response curves obtained over a series of several imaging sessions for the four field PAG gel dosimeter at a temperature of 4°C. For all images, the CT imaging protocol was employed (refer to section 4.1.5). Error bars represent the standard deviation in the average dose measured in regions of interest. Error in <i>N_{CT}</i> , not illustrated, is $\pm 0.5 N_{CT}$ for all data points.	
Figure 4.15	75
Comparison of the average <i>N_{CT}</i> – dose response of the four field PAG gel dosimeter obtained at two different gel temperatures. A shift in <i>N_{CT}</i> and a small change in the slope of the response are observed between the two results. For all images, the CT imaging protocol was employed (refer to section 4.1.5). Error bars represent the standard deviation in the average dose measured in regions of interest. Error in <i>N_{CT}</i> , not illustrated, is $\pm 0.5 N_{CT}$ for all data points.	
Figure 4.16	77
Comparison of CT and MR image data illustrating excellent agreement in localization of the high dose region in the four field gel used in this study. The plot shows a 1D profile along the length of the 6Gy beam from entrance to exit. A 3x3 median filter has been applied to the CT data.	

ACKNOWLEDGMENTS

I would like to thank several people who, through their support, encouragement and help have made completion of this thesis possible and, most importantly, enjoyable. Foremost, my supervisors, Dr. Chantal Audet and Dr. Cheryl Duzenli, have been excellent. Despite their hectic clinical workload, they have been continually responsive to my questions and ideas. The combination of expertise, support and freedom they have offered me has been perfect. I look forward to working in our gel group during the next year!

Many people in the medical physics department at the Vancouver Cancer Centre has somehow supported this work. Thank you for the discussions, practice talk sessions, computer help, advice, sharing of clinical experience and coffee breaks! Of special note are my fellow medical physics students who, by creating a group atmosphere, have made this work fun. Thanks James, Shevonne, Bilal, Leah, Troy and Andrew for the discussions, ears for my gripes and triumphs, programming help (James!) and laughs.

The support I receive from my family is unyielding. Mom and Dad, thank you for believing I could accomplish anything I put my heart and mind to. Janet, thank you for continually introducing me to alternatives.

Finally, thanks to Drew. His constant friendship and unbelievable ability to reduce my stress are irreplaceable.

I would also like to gratefully acknowledge financial support from the National Science and Engineering Council of Canada in the form of a PGS A Scholarship and the British Columbia Cancer Agency.

CHAPTER 1

INTRODUCTION

Radiation therapy, the treatment of disease by radiation, is used to treat 45-50% of all patients requiring treatment for cancer in Canada. Considering cancer is the leading cause of death for Canadians, and 129,200 new cancer cases were estimated in Canada in 1998, radiation therapy plays a large and important role in Canada's health care system today (Nat. Cancer Institute, 1998).

Conventional radiation therapy uses photon or electron radiation of various energies to treat patient tumours. Radiation beams are most commonly delivered by a medical LINear ACcelerator (LINAC). The gantry of a LINAC can rotate 360° about a single point in space called the isocenter (see Karzmark, 1984, for a complete description of a LINAC). An isocentric patient set-up involves placing the tumour volume at the isocenter such that multiple beams entering the patient from various angles can intersect at the tumour (Johns and Cunningham, 1983). As a result, the tumour receives a high dose while the entrance dose to the surrounding tissues is minimized.

Of primary concern in radiation therapy is the accurate determination of the amount and distribution of radiation, or dose, delivered to a patient during a radiation treatment. (For a discussion of dosimetry, see section 2.1). In radiotherapy clinics computerized treatment planning systems are used to calculate the dose delivered to the tumor and surrounding tissues as well as to custom design the arrangement of beams to achieve the prescribed dose

to the patient tumour volume. Typical treatment planning systems use calculation algorithms that require measured data characterizing each of the radiation beams used in the clinic.

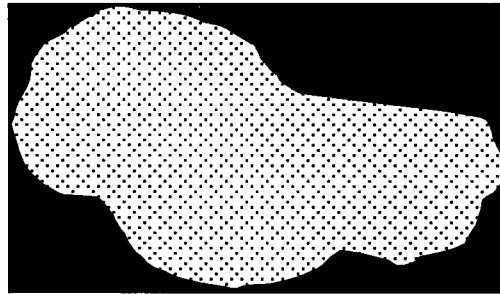
To provide beam data for input into the treatment planning system, or to commission the beam, dose measurements are made directly from the radiation beam. Dosimeters, instruments that provide readings related to the absorbed dose deposited in their sensitive volumes (Johns and Cunningham, 1983), are used to perform these measurements. Aside from beam commissioning, dosimeters are also commonly employed to perform standard beam calibration and quality control measurements and to verify, through measurement, the dose calculations produced by the treatment planning system.

Polymer gel dosimeters (Maryanski *et al*, 1993) are new dosimeters now under development for use in radiation dosimetry. These dosimeters provide many novel advantages over standard dosimeters used in radiation therapy. In particular, their ability to store dose distributions in 3D is valuable for verifying treatment planning dose calculations since tumours, and the dose volumes resulting from treatments, are inherently 3D (Battista *et al*, 1996, Olsson *et al*, 1998).

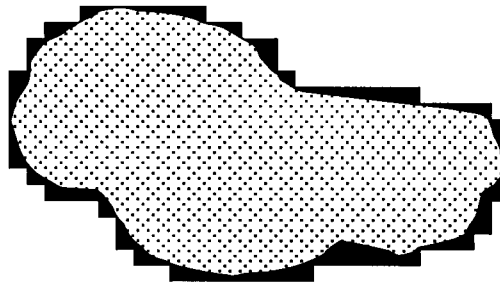
In a polymer gel dosimeter a spatially retained chemical change records locally absorbed dose. The dose information is extracted from the irradiated gel using an imaging technique. Traditionally, MRI has been used to image the gel, but given the inaccessibility and expense of MRI scanners, widespread clinical implementation of this new dosimetry technique has been impeded. This thesis investigates the potential of using another, more accessible imaging technique, x-ray computed tomography (CT), to perform polymer gel dosimetry.

1.1 Motivation for a 3D Dosimeter

Radiation therapy involves a continual compromise between delivering the prescribed dose to the tumor and introducing complications for the patient due to radiation absorbed by surrounding healthy tissues. This compromise is particularly evident when a tumor is in close proximity to a critical organ. In efforts to reduce dose to the surrounding tissue, techniques are being increasingly employed that aim to conform the high dose volume closer to the tumor volume. These techniques are referred to as conformal radiotherapy techniques. Figure 1.1 schematically illustrates the dose sparing to surrounding tissues that can result from implementing conformal techniques.



1.1a



1.1b

Figure 1.1 An illustration of dose sparing as a result of conformal radiotherapy. Figures 1.1a and 1.1b show examples of the type of high dose region (represented in black) resulting from, respectively, a typical four field treatment and a multi-leaf collimator conformal treatment. Greater sparing of healthy tissue from high doses is evident with the conformal treatment. The cross-hatched area represents the clinical target volume (ICRU 50, 1993).

Conformal radiation therapy is a 3D process. Patient anatomy, as well as the size, shape and position of the tumour, are defined by 3D image sets (Robb, 1998). Modern treatment planning systems provide a platform for planning radiation treatments in 3D using the 3D CT image sets (Dobbs and Webb, 1988) and algorithms capable of calculating dose in 3D. The 3D image sets and dose calculation algorithms allow for 3D, or non-coplanar, beam delivery. The 3D high dose volume may be conformed using dynamic multi-leaf collimation (MLC) and intensity modulated radiation therapy (IMRT). MLC is used to conform the high dose volume to the clinical target volume by shaping the beam on each beam's eye view. IMRT conforms the high dose volume by allowing the beam intensity to vary across the treatment field. Both MLC and IMRT can provide highly irregular 3D high dose volumes.

To accurately measure the irregular dose distributions resulting from conformal treatments a dosimeter that can measure dose in 3D with a high spatial resolution is required. These measured 3D dose distributions can then be compared to the distributions calculated by the treatment planning system. Such a comparison allows for verification of the accuracy of delivery of the prescribed dose to the tumour volume and establishes the limitations and accuracy of the treatment planning algorithms.

1.2 Standard Dosimeters and Dose Measurement in 3D

Many different types of dosimeters are frequently used in radiation therapy clinics. Most are not tissue equivalent and since absorbed dose depends highly on the absorbing material (see section 2.1 for more information on dosimetry), the dosimeter must be placed in a material deemed to be tissue equivalent with respect to its ability to absorb dose. Such

materials include water, solid water[®], lucite and perspex. The tissue equivalent material in which dose measurements are made can be constructed in regular or irregular shapes to simulate either standard reference conditions or body contours, and is called a phantom. The most common dosimeter is the ionization chamber. Others include thermoluminescence detectors (TLDs), diodes, calorimeters, radiographic film and chemical dosimeters (Johns and Cunningham, 1983). Each of these devices has advantages and disadvantages that encourage its use in particular situations and discourage it in others. The following briefly covers the potential for these dosimeters to measure 3D dose distributions.

Ionization chambers and diodes measure the dose deposited in small sensitive volumes (Johns and Cunningham, 1983, Khan, 1984). Ion chambers are frequently used to calibrate and commission radiation beams. In order to measure a treatment dose with a high spatial resolution in a large, irregular 3D phantom, ionization chambers or diodes would have to be placed at many points throughout the phantom or scanned in many directions. Furthermore, the entire irradiation treatment would have to be repeated for each point which is far too time consuming to be practical.

TLD dosimeters also measure dose at a point; however, several TLDs may be positioned simultaneously in a 3D grid of points machined out of a tissue equivalent material in order to achieve dose measurement in 3D. Compared to ionization chambers and diodes, as mentioned above, this technique would require fewer repeat irradiations. The spatial resolution of the grid would be limited by the size of the TLDs (~1mm) and the fact that most TLDs are not tissue equivalent and therefore cannot be placed closely together without perturbing the distribution of dose. Since absorbed dose due to ionizing radiation is highly

dependent on the absorbing material (see section 2.1), tissue equivalence is desirable for dosimetric measurements. Also, the response of each TLD to dose will change unpredictably over time requiring repeated calibration of each TLD before each use (Johns and Cunningham, 1983). Since many TLDs are required to fill the grid, bookkeeping and calibration of all the TLDs would be tedious and time consuming.

Radiographic film is a high resolution two dimensional (2D) dosimeter (Johns and Cunningham, 1983). It can measure dose in 3D by stacking 2D information. The spatial resolution in the vertical (or stacking) direction is defined by the thickness of phantom material between each sheet of film. Resolution is therefore compromised, as with TLDs, by the presence of film in high densities destroying the tissue equivalence of the phantom. Also, the dose-response of film depends on photon energy and usually has to be calibrated for different depths since photon energy is affected by depth in the phantom. Calibrating for all depths would make 3D film dosimetry tedious as well. A promising new 2D film dosimetry technique involves radio-chromic film which, although very expensive, is tissue equivalent and responds to dose independently of photon energy (Niroomand-Rad *et al*, 1998, Ramani *et al*, 1994).

A chemical dosimeter, such as the Fricke dosimeter, records absorbed dose by measuring radiation - induced chemical changes in an aqueous solution (Johns and Cunningham, 1983). Most chemical dosimeters are liquid and can be used to measure dose in volumes of any shape, but, due to ion diffusion, no spatial information within that volume is retained.

It is evident that traditional dosimeters do not provide an adequate means of measuring dose in 3D with high spatial resolution. Dosimetry techniques employing

polymer gels provide such a means. The gels not only store dose in 3D, but are tissue equivalent and hence can act as both the dosimeter and the phantom.

1.3 A Brief History of Gel Dosimetry

The following is a brief history of the research leading to the development of the polymer gel dosimetry technique. Nuclear magnetic resonance (NMR) methods were introduced in 1984 to extract dose information from Fricke chemical dosimeters (Gore *et al*, 1984a). When a Fricke dosimeter is irradiated, ferrous ions (Fe^{2+}) in an aqueous solution are oxidized to form ferric (Fe^{3+}) ions in proportion to absorbed dose. It was found that the NMR spin-lattice relaxation rate (R_1) for water protons in the Fricke solution, which depends on the concentration of Fe^{3+} ions, is proportional to the dose absorbed by the solution (Gore *et al*, 1984a). The spin-lattice relaxation rate provided a novel means of obtaining dose information from the irradiated dosimeter. However, this dosimetry technique could not be used to measure 3D dose distributions since ions are free to move within the aqueous medium and the spatial dose information is not maintained.

In an effort to maintain the spatial dose distribution, an agarose gel was infused with the Fricke solution resulting in the Fricke gel dosimeter (Gore *et al*, 1984b, Schulz *et al*, 1990). The gel limited the ion diffusion such that MR images obtained shortly after irradiation of the gel could provide spatial dose information. Unfortunately, the ions could still diffuse slowly over time and the spatial dose information was eventually lost (Maryanski *et al*, 1993).

A new gel dosimeter was later introduced (Maryanski *et al*, 1993) in which an aqueous gel was infused with monomers that polymerized and crosslinked (details of this process are found in section 2.2) when the gel was irradiated. As with the Fricke gel, this polymer gel was analysed for dose information using MRI. It was found that dose contrast exists in MR images of irradiated polymer gels mainly because the NMR properties of water protons hydrating polymer are different from those of water protons hydrating monomer (Audet, 1995). In particular the NMR spin-spin relaxation rate (R_2) was found to vary linearly with absorbed dose.

This new polymer gel dosimeter proved to have many advantages over the Fricke gel dosimeter. Most importantly, it had the ability to retain a spatial dose distribution indefinitely. Possible explanations are that the crosslinked polymer molecules are too large to diffuse through the gel matrix, or they become entangled in or react with and become attached to, the gel matrix. The composition of this original polymer dosimeter, the BANANA gel, was bisacrylamide (Bis), acrylamide, nitrogen, and agarose. With further studies, the composition was changed by replacing agarose with gelatin. The advantage of using gelatin was that a greater dynamic range of dose could be measured. The new adapted polymer gel, composed of Bis-acrylamide, Acrylamide, Nitrogen and Gelatin was hence termed BANG[®] gel (Maryanski *et al*, 1994). Other formulations of polymer gels have since been developed by MGS Research Inc. – BANGII and BANGIII. The work in this thesis employs polymer gels of the original BANG[®] formulation, but will be referred to as PAG (PolyAcrylamideGelatin) gels because since 1998, BANG[®] has been a registered trademark of MGS Research Inc. reserved for the gels procured from that company.

Recent research demonstrates that the PAG gel dosimeter has many standard characteristics required for a successful dosimeter: accuracy, precision, sensitive response to dose, stability over time, tissue equivalence, integration of dose over duration of treatment, a dose response independent of dose rate and energy and a linear response to dose (Audet, 1995, Maryanski *et al*, 1996a, Ibbott *et al*, 1997). It is however uniquely valuable in its ability to record, with high spatial resolution, complete integrated 3D dose distributions produced by modern treatment techniques (Maryanski *et al*, 1996a, Ibbott *et al*, 1997). Such treatments include stereotactic radiotherapy, Gamma Knife[®] treatments and high-dose-rate brachytherapy, or involve dynamic wedge, intensity modulation and complex field shapes produced by multi-leaf collimators. Preliminary results also suggest that the PAG gel dosimeter has potential for producing high spatial resolution dose maps for heavy particle beams such as a proton beam (Maryanski *et al*, 1996a).

Alongside this ability to measure 3D dose distributions, the PAG gel dosimeter is also unique in that it can be prepared in containers that take the shape of parts of the human body (Kaurin *et al*, 1999, Pfaender *et al*, 1999, Hepworth *et al*, 1999, Gustavsson *et al*, 1999). The gel container can be constructed to mimic tissue inhomogeneities and hence, using PAG gel, anthropomorphic phantoms can be constructed that model different structures within the patient, such as bones or lungs. This is a valuable characteristic since accurate dose measurements can be made that take into account tissue inhomogeneities. PAG gel is also unique in that the dosimeter is the phantom. This is in contrast to non-tissue equivalent traditional dosimeters which must be kept thin, small and well - spaced in order to probe dose at points or planes in a tissue equivalent phantom.

1.4 Motivation for X-ray Computed Tomography Gel Dosimetry

A factor impeding the implementation of MRI gel dosimetry in clinical radiation therapy is the inaccessibility of MRI scanners in many radiation therapy departments. Without easy and reliable access to an MRI scanner, MRI gel dosimetry, as an everyday means of verifying complicated conformal treatment plans, is not feasible. MRI scanners will not likely become an integral component of radiation therapy departments for some time and therefore, if gel dosimetry is to be implemented clinically on a large scale, another way of extracting the dose information from the gel will have to be employed.

A new method under development involves extracting the dose information from polymer gel using optical computed tomographic densitometry (optical CT), and exploiting the optical changes observed in PAG gel upon irradiation. A prototype optical scanner has been developed that uses a He-Ne laser to scan across the gel during each incremental rotation as the gel rotates on a platform. Using photodiode detectors, a set of optical density projections are measured and then reconstructed to form a cross-sectional image of optical density in the gel (Gore *et al*, 1996). The optical density of an irradiated gel depends on the production of light-scattering polymer micro-particles at the sites of radiation absorption. The light scattering from these particles produces an attenuation of transmitted light that is directly proportional to the absorbed dose. It follows that a cross-sectional image of the gel's optical density is related to absorbed radiation dose (Maryanski *et al*, 1996b). Optical CT is also being developed as a means of extracting dose information from another type of gel dosimeter, ferrous-benzoic-xyleneol (FBX) gel dosimeter (Kelly *et al*, 1998).

An optical CT system can be constructed at relatively low cost and is therefore a potential solution to making gel dosimetry more accessible to radiation therapy clinics. However, although promising, this technique requires a device not currently available to radiation therapy departments and has inherent limitations such as a requirement that gel vessels be cylindrical in order to allow reconstruction algorithms to correct for refraction at interfaces in the gel (Gore *et al*, 1996). Recently preliminary investigations have shown that Raman spectroscopy of PAG gels can provide dosimetric information (Baldock *et al*, 1998).

Polymer gel not only exhibits an optical density change upon irradiation, but also a physical density change. Since x-ray computed tomography (CT) produces images based on changes in the attenuation coefficient and hence changes in density in different materials, the possibility exists of using x-ray CT to extract dose information from irradiated gels. This possibility is exciting in that CT scanners are easily accessible to radiation therapy departments and CT gel dosimetry could be implemented for everyday clinical use. Also, since CT images are used in designing treatment plans for patients, CT images of measured doses could easily be co-registered to the treatment planning CT images used to calculate the doses. Once images are co-registered, the measured and calculated dose distributions can be automatically overlaid for simple comparison.

The purpose of this thesis is to investigate the feasibility of using x-ray CT for performing polymer gel dosimetry. In Chapter Two, some background information pertinent to the investigation is presented. This includes a brief introduction to the theory of radiation dosimetry followed by a discussion of how radiation interacts with PAG gel and then a presentation of the theory and practical issues surrounding x-ray computed tomography (CT). In Chapter Three the materials and methods used in the experiments are described. This

includes an introduction to the techniques used in gel preparation, irradiation, CT imaging and image processing. In Chapter Four the results of this investigation are presented and discussed. The development of a protocol for CT imaging PAG gels that provides images with the highest possible dose contrast and spatial resolution is described first. Then, the results of investigating the nature and reproducibility of the dosimeter's CT number – dose response are presented. This is followed by a comparison between CT and MRI methods for extracting dose information from PAG gels. In the last section of Chapter Four, quantitative determinations of the density changes occurring in PAG gel are presented. In Chapter Five the main conclusions of this work are summarized.

CHAPTER 2

BACKGROUND INFORMATION

Presented in this chapter is some background information related to the investigation of using x-ray computed tomography for performing polymer gel dosimetry. First, a brief introduction is given to the theory of radiation absorbed dose and the clinical dosimetry of photon and electron beams. This is followed by a discussion of the chemical reactions induced by radiation in PAG gel that result in the ability of a PAG gel to record absorbed radiation dose. Finally, an introduction to x-ray computed tomography (CT) is provided.

2.1 Radiation Dosimetry Theory

A comprehensive review of radiation dosimetry theory is well beyond the scope of this thesis and the reader is referred to Johns and Cunningham (1983), Attix (1986) or Khan (1994) for a detailed analysis. The following is a brief review, drawn from these texts, of some of the main concepts in radiation dosimetry that are relevant to this investigation. The concept of absorbed dose is introduced, and the clinically relevant photon and electron interactions with matter are discussed in section 2.1.1. The clinical measurement of radiation dose (dosimetry) is discussed in section 2.1.2 and the difference between relative and absolute dosimetry is described in section 2.1.3.

2.1.1 Radiation Absorbed Dose

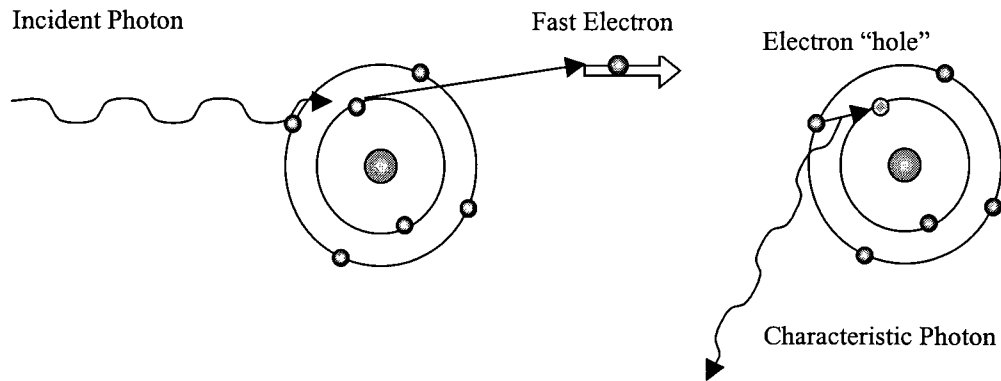
Ionizing radiation deposits energy in matter by interactions that result in excitation or ionization of atoms or molecules. A quantity called absorbed dose is used to measure the

energy absorbed by matter and is defined as the amount of energy absorbed in a medium per unit mass. Absorbed dose is given in SI units, J/kg or Gray (Gy). Since a particle passing through matter must carry charge in order to excite and/or ionize atoms or molecules, photons, which are uncharged, deposit dose indirectly by transferring their energy to electrons which can then deposit some of this energy as dose. Some energy will be lost by radiative processes later. Photons are therefore termed indirectly ionizing radiation and electrons directly ionizing radiation. Since photon and electron beams are the most common in radiation therapy clinics (LINACs produce both types of beams) their interaction with matter is discussed here.

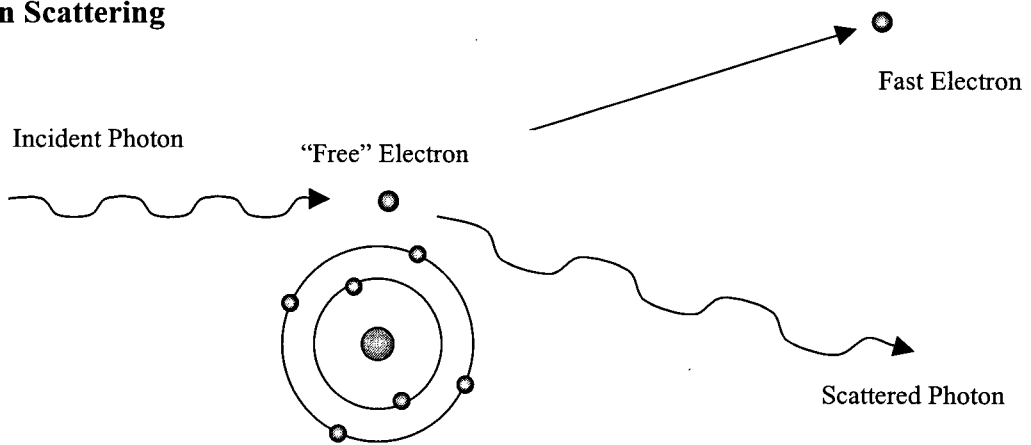
Photons

Photons at clinically relevant energies ($\sim 40 \text{ keV} \Rightarrow \sim 20 \text{ MeV}$) interact with matter in three main ways that result in dose absorption: photoelectric effect, Compton scattering and pair production. Figure 2.1 schematically illustrates these three photon interactions. In the photoelectric effect an incident photon interacts with, and transfers its energy to, a bound atomic electron. The result is a fast electron that causes ionizations and excitations leading to absorbed dose. If the photon interaction occurs with an inner bound electron, characteristic x-rays are given off when an outer electron moves in to fill the hole created in the inner shell. Compton scattering is the interaction of a photon with an outer shell electron that has a binding energy much less than the photon energy so that the electron can be considered "free". In this interaction some of the photon's energy is transferred to the electron and the photon scatters with the remaining energy. Pair production occurs when an incident photon, interacting with the field of a nucleus, produces an electron – positron pair and disappears. The positron, surrounded by electrons, is however short lived and annihilates with a nearby

Photoelectric Effect



Compton Scattering



Pair Production

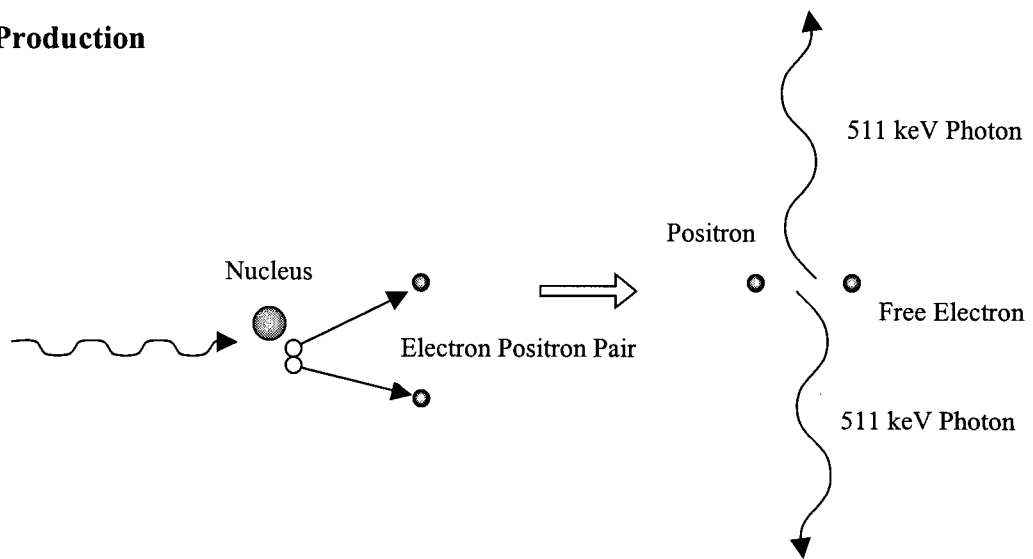


Figure 2.1 Schematic illustration of the three interactions of photons with matter that are important for dose deposition in tissue.

electron. This produces two back to back 511 keV photons. There is a threshold energy of 1.022 MeV required for pair production (twice the electron rest mass energy). Any excess photon energy is transferred to kinetic energy of the electron and positron pair.

The three photon interactions just described occur with probabilities that depend on photon energy and atomic number of the absorbing medium. The photoelectric effect is predominant only at low energies (< 100 keV) and has a probability of occurrence that increases with atomic number as $\sim Z^3$. The probability of Compton scattering decreases with increasing energy, but is independent of atomic number. Pair production becomes dominant only at high energies (> 1.022 MeV) and occurs with greater probability as photon energy and atomic number increase.

The amount of attenuation of photons resulting from these interactions is determined by the linear attenuation coefficient, μ (cm^{-1}), of the material such that the fraction of photons transmitted is given by:

$$\frac{I}{I_o} = e^{-\mu x} \quad (2.1)$$

where I_o is the initial beam intensity, I is the beam intensity beyond a thickness of the material x , and μ is the attenuation coefficient. A linear absorption coefficient is also defined, μ_{ab} , that determines the fraction of photon energy absorbed by the material rather than lost by radiative processes. Furthermore, a mass absorption coefficient is defined:

$$\frac{\mu_{ab}}{\rho} \quad (\text{cm}^2/\text{g}) \quad (2.2)$$

where μ_{ab} is the linear absorption coefficient and ρ is density. Using this mass absorption coefficient, absorbed dose, D , is defined as:

$$D = \Phi \left(\frac{\mu_{ab}}{\rho} \right) \quad (2.3)$$

where Φ is the energy fluence (MeV/m²) of the initial beam and $\frac{\mu_{ab}}{\rho}$ (cm²/g) is the mass absorption coefficient (Johns and Cunningham, 1983).

Electrons

As briefly mentioned, electrons traveling through a medium lose energy through collisions with atoms, causing ionizations and excitations, or through radiative interactions. Excitations occur when an atomic electron, experiencing the field of the incident electron, gains energy and is excited. If the energy gained is greater than the binding energy, the electron can be ejected completely from the atom, ionizing the atom and producing fast, secondary electrons. Radiative interactions occur when electrons, interacting with nuclear fields in the medium, decelerate and emit photon energy. Bremsstrahlung (German for braking radiation) is the term applied to this process. The total electron energy lost (E_{tot}) by both collisional and radiative processes is quantified by the total linear stopping power, (S), defined as kinetic energy lost per unit path length traveled by an electron in a medium (dE/dx). The total stopping power (S_{tot}) is the sum of the collisional (S_{col}) and radiative (S_{rad}) stopping powers. Absorbed dose is related to S_{col} since S_{col} describes the electron energy transferred to the medium that results in excitations and ionizations and can be defined as:

$$Dose = \int \frac{1}{\rho} \left(\frac{dE}{dx} \right)_{col,\Delta} \Phi dE \quad (2.4)$$

where $\frac{1}{\rho} \left(\frac{dE}{dx} \right)_{col}$ is mass collisional stopping power (Khan, 1994). It is these excitations and ionizations resulting from energy transferred to the medium that produce the biologically significant effects that we attribute to absorbed radiation dose.

2.1.2 Clinical Dosimetry

As discussed above, absorbed dose depends on the absorbing medium. For this reason, dose measurements must be made in a tissue or water equivalent material called a phantom (see section 1.2). For megavoltage photon beams (for which the Compton effect dominates) only the electron density of a material need match that of water in order to be considered tissue equivalent. For megavoltage electron beams the electron density and the atomic number, Z , must be matched.

However, even when dose measurements are performed in a tissue equivalent phantom, care must be taken when making dose measurements using a dosimeter that is not tissue equivalent. This is because a non-tissue equivalent dosimeter can perturb the dose delivered to the phantom (by, for instance, changing the amount of scattered radiation). When performing absolute dose measurements to calibrate the output of a LINAC at a point, ion chambers are typically used. The perturbations of these non-tissue equivalent dosimeters on the measured dose must be accounted for using a well defined protocol (Task Group 21, 1983) developed by the American Association of Physicists in Medicine. This protocol consists of the application of many correction factors in order to determine absorbed dose to tissue from measurements made using a non-tissue equivalent chamber in a water phantom. Although this protocol makes every effort to issue accurate and consistent dosimetric results, the many numerical corrections required is a factor increasing uncertainty in absolute

dosimetry (Jayaraman *et al*, 1985, Harrison, 1993). Although PAG gel dosimetry is being developed to characterize 3D dose distributions with a high spatial resolution rather than to perform precise absolute calibrations at a point, the above example illustrates the benefits of the tissue equivalence of PAG gel.

2.1.3 Relative and Absolute Dosimetry

Relative Dosimetry

Relative dosimetry is concerned with determining the values of dose at distributed points in a medium relative to a reference point in that medium, commonly the point of maximum dose. One can determine actual dose values throughout the volume of interest by means of a suitable calibration curve (dose response curve). If the dose response of a dosimeter is linear for the range of doses measured, then relative doses are obtained merely from the ratio of dosimeter measurements above a background (0 Gy) reading, without the need to determine the actual dose to any point. This is illustrated in the following:

If,

$$M_1 = a D_1 + b, \text{ and likewise, } M_{max} = a D_{max} + b \quad (2.5)$$

where M is a dosimeter reading, D is dose and $b = M(0 \text{ Gy})$,

then,

$$\frac{\Delta M_1}{\Delta M_{max}} = \frac{M_1 - b}{M_{max} - b} = \frac{aD_1}{aD_{max}} = \frac{D_1}{D_{max}}. \quad (2.6)$$

Clearly, linearity of the ΔM – dose response is required to carry out relative dosimetry in this way, however, reproducibility of the slope of the dose response curve (the sensitivity) is not required.

Given a linear N_{CT} -dose response for the CT PAG gel dosimetry technique, the dose resolution for (or uncertainty in) relative dose measurements can be determined as follows. As shown in Equation 2.6, a dose measurement relative to the maximum dose (D_{max}) is given by:

$$\%x = 100 \times \frac{\Delta M_x}{\Delta M_{max}} \quad (2.7)$$

where ΔM_{max} and ΔM_x are measurements, above background, made at the point of maximum dose and at an area of interest, respectively. Standard error propagation rules show that given $a = a \pm \sigma a$, and $b = b \pm \sigma b$, the uncertainty in $y = ab$ is given by:

$$\sigma y^2 = \left(\frac{\partial y}{\partial a} \right)^2 \sigma a^2 + \left(\frac{\partial y}{\partial b} \right)^2 \sigma b^2. \quad (2.8)$$

Thus, a relative dose measurement as given in Equation 2.7, has an associated uncertainty, or dose resolution, given by:

$$\sigma_{\%x} = \sqrt{\sigma_{\Delta M}^2 \left(\frac{100}{\Delta M_{max}} \right)^2 + \sigma_{\Delta M_{max}}^2 \left(\frac{-100 \Delta M}{\Delta M_{max}^2} \right)^2} \quad (2.9)$$

Given a reproducible linear N_{CT} -dose response for the CT PAG gel dosimetry technique, the dose resolution for actual dose measurements can be determined as follows. For a linear N_{CT} -dose response, an actual dose measurement is given by:

$$D = \frac{\Delta N_{CT}}{m}, \quad (2.10)$$

where ΔN_{CT} is N_{CT} measured above background (0 cGy) and m is the slope of the N_{CT} -dose response curve. Thus, from standard error propagation rules (see Equation 2.8), the

uncertainty in this actual dose measurement, or the dose resolution when making actual dose measurements, is given by:

$$\sigma_D = \sqrt{\sigma_{\Delta N_{CT}}^2 \left(\frac{1}{m}\right)^2 + \sigma_m^2 \left(\frac{-\Delta N_{CT}}{m^2}\right)^2} . \quad (2.11)$$

Absolute Dosimetry

Absolute dosimetry is the process of accurately determining dose to a reference point in a reference medium and is far more challenging than relative dosimetry. This reference point dose can then be used to cross - calibrate other dosimeters for use in relative dosimetry. For absolute dosimetry one uses an established fundamental theoretical model to relate dosimeter readings to dose. Examples of absolute dosimeters include calorimeters and Fricke chemical dosimeters. The PAG gel dosimetry technique described in this thesis is not an absolute dosimetry technique since the fundamental relationship between the observed changes in the gel and the energy absorbed have not yet been established.

2.2 PAG gel and Radiation Reactions

The PAG gel responds to radiation briefly as follows. Irradiation of the gel results in the production of free water radicals. These radicals react with molecules in the gel initiating chemical reactions at the site of radical formation. The amount of reaction product is generally proportional to the number of free radicals produced and hence to the dose absorbed locally in the gel. In the following discussion details of this general description are provided.

2.2.1 Water Radiolysis

The PAG gel is approximately 90% water by weight. (The composition by weight optimizing the gel's response to radiation was shown to be 5% gelatin, 3% acrylamide and 3% Bis (Audet, 1995).) As a result, radiation incident on the gel is primarily absorbed by water.

The interaction of ionizing radiation with water, termed water radiolysis, is a well studied subject found in any radiation chemistry text such as that by A.J. Swallow (1973). A detailed discussion of water radiolysis is beyond the scope of this thesis. It is sufficient to know that water radiolysis results in the production of the free radicals: e^-_{aq} , $OH\bullet$ and $H\bullet$, (where \bullet means active radical), and that these radicals initiate chemical changes in the PAG gel.

2.2.2 Radical Chain Polymerization

A polymer is a molecule consisting of repeating molecular units called monomers. The process by which monomers join to form polymers is termed polymerization. Water radicals initiate the polymerization of monomers present in PAG gel. Polymerization involving two monomers instead of one is termed co-polymerization. Due to ease of notation only, the following discussion refers to polymerization.

There are two kinds of polymerization: step polymerization and chain polymerization. In step polymerization groups of monomers have similar reactivity to that of single monomers such that the groups can join together to form much larger polymers or a single monomer can join a group, increasing the length of the polymer by one monomer. In this fashion the polymer grows in steps of any number of monomers.

In chain polymerization a reactive center is initially formed on a monomer that will react with other monomers in such a way that this center is maintained and can continue to react with monomers. The polymer hence grows one monomer at a time (as if adding links to a chain). Chain polymerization can proceed via radical initiation, anionic initiation, cationic initiation or by coordination catalysis. The first three methods all involve an initiator that creates the reactive center by reacting with a monomer. Coordination catalysis is unique in that a true catalyst acts to create the active center (Boyd and Phillips, 1993).

Upon irradiation, the acrylamide and Bis-acrylamide undergo radical chain polymerization (Hsu and Cohen, 1984). The sequence of steps involved in this process is initiation, propagation and termination. The initiation step produces an active monomer and is described by:



where $I\bullet$ is a free radical product of water radiolysis, M represents a monomer, and $M\bullet$ is a monomer with a reactive center. Note that in this discussion M represents either the acrylamide or Bis monomer in the PAG gel.

In the second step, propagation, an active monomer (or monomer chain) reacts with a single monomer to increase the chain length by one monomer. The result is a reactive monomer chain. This step may be represented as follows:



where the subscripts on M_n and M_{n+1} represent the number of monomers in the chain.

The final step, termination, results in an inactive polymer. Termination can occur by either recombination or disproportionation. Recombination is simply two active ends

combining directly to form a bond joining two active chains into one inactive polymer.

Recombination is described by:



Disproportionation is less obvious but competitive with recombination in terminating polymerization. It results from the active end of one monomer chain pulling a hydrogen ion from the reactive center of another monomer chain, producing two inactive polymers.

Disproportionation is described by:



(Boyd and Phillips, 1993).

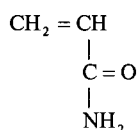
2.2.3 *Polymerization and Crosslinking in the PAG gel*

The monomers in the PAG gel dosimeter are acrylamide and N,N'-methylenebisacrylamide (Bis). These molecules undergo free radical chain polymerization to produce cross-linked polyacrylamide when double bonded carbons break creating reactive centers on the monomers. Acrylamide, with a single double bond (see Figure 2.2), forms linear polymer chains. Bis, with two double carbon bonds (see Figure 2.2), introduces active network points to the already formed linear polymers. This results in branched polymer molecules and is termed crosslinking. Bis is known as a crosslinker for acrylamide.

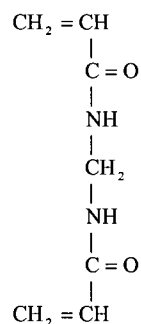
The cross-linked polyacrylamide that is formed from acrylamide and Bis can be essentially infinite in size and cannot be dispersed molecularly in solvent. The presence of Bis is necessary in the PAG gel in order to produce these large branched polymers that cannot diffuse through the gel matrix. Bis is also necessary for giving the gel an NMR and optical response to dose (Maryanski, 1993 and 1996b).

Acrylamide and Bis are given by the chemical formulae $\text{CH}_2\text{:CHCONH}_2$ and $(\text{CH}_2\text{:CHCONH})_2\text{-CH}_2$, respectively. The chemical structures of these monomers and of the radiation product, cross-linked polyacrylamide, are shown in Figure 2.2 (Audet, 1995). The crosslinking role of Bis is clearly visible in the chemical structure of cross-linked polyacrylamide. This branching structure allows polymerization, and hence the record of absorbed dose, to be maintained spatially within the gel.

Acrylamide:



Bis:



Crosslinked Polyacrylamide:

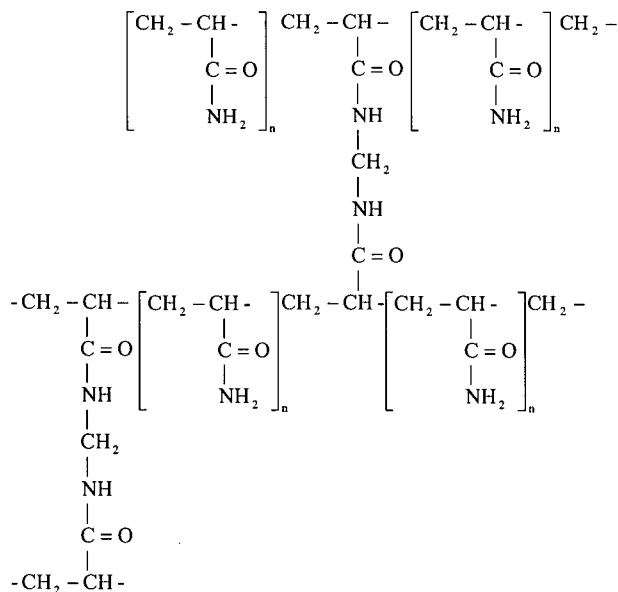


Figure 2.2 The chemical composition of acrylamide, N,N'-methylenebisacrylamide (Bis) and cross-linked polyacrylamide.

Oxygen is an inhibitor of the radiation - induced polymerization in the PAG gel, described above. Oxygen inhibits the propagation of polymerization by combining with the reactive monomers and rendering them relatively inactive (Bio.-Rad. Bulletin, 1987). Thus, oxygen must not be introduced during the preparation of PAG gel otherwise polymerization will not take place. Also, if the amount of oxygen varies between gels, their responses to dose will be inconsistent and irreproducible. Another factor to consider is diffusion of surrounding oxygen into a gel purged of oxygen. Glass containers or plastic containers with a wall thickness of at least 5 mm prevent oxygen from entering the container from the outside. With plastic containers there remains the risk, however, of oxygen trapped in container walls diffusing into the gel (Maryanski *et al*, 1994). In order to remove this risk the plastic containers are irradiated prior to use to purge them of oxygen content.

Polymerization reactions of acrylamide and Bis in PAG dosimeters are also affected by the presence of gelatin. Gelatin functions to moderate the radiation response, resulting in a constant polymer yield with dose as opposed to a step function response with dose (Maryanski, 1993). This in turn provides the linear response of R2 to dose observed in MRI polymer gel studies. Increasing the amount of gelatin has been shown to decrease the polymer yield. It appears though, that gelatin has little effect on the NMR relaxation properties of the polymer which suggests that the structure and composition of polymer are not affected by gelatin (Audet, 1995).

2.3 X-ray Computed Tomography

The first patient scanned using x-ray computed tomography in 1972 was a woman suspected of having a brain lesion. The image of her brain illuminated a dark circular cyst

(Hounsfield, 1980). Since that time x-ray computed tomography has come to revolutionize medical imaging in its ability to provide soft tissue contrast (compared to traditional x-rays) and provide 3D anatomical information in a digital format. Presented in this section is an introduction to x-ray computed tomography. Conventional x-ray imaging and its limitations is described in section 2.3.1 and in section 2.3.2 is described how a modern x-ray computed tomographic scanner operates and produces images that overcome these limitations. This is followed by a description of the image output, CT numbers, in section 2.3.3 and the relationship between CT number and density in section 2.3.4. The final section, 2.3.5, is an introduction to some sources of noise and reduced resolution.

2.3.1 Conventional Imaging with X-Rays

X-ray computed tomography is related to conventional x-ray imaging, or radiographic imaging, the most common form of medical imaging used today. A radiographic image is formed by photons passing through a patient and interacting with a photon detector on the other side of the patient. A radiograph is therefore an image of photons transmitted through the patient.

Photons arriving at the detector (often film) are photons coming directly from the source and that pass straight through the patient (primary photons) or scattered photons that are the result of interactions within the patient (secondary photons). Since secondary photons are incident on the detector from any direction, they do not contain any useful dose information and contribute to noise. Anti-scatter grids are positioned between the patient and the detector in efforts to reduce this source of image noise. Primary photons that reach the detector carry useful information about the probability of a photon being transmitted along a particular line through the patient. This probability is determined by the photon attenuation

properties of the tissues through which the photon travels and hence differentiates tissues, especially soft tissues from bone (Curry, 1990).

There are two important limitations to conventional radiography: poor soft tissue contrast and loss of depth information.

1) Poor soft tissue contrast

Conventional x-ray films are sufficient for visualizing structures with contrasting densities. For example, ribs or an air filled trachea are clearly distinct from surrounding soft tissues on x-ray films. However, to visualize soft tissue details, such as blood vessels or heart tissues, a conventional radiograph is of limited use.

2) Loss of depth information

In a conventional x-ray, the information from a 3D object (the body) is projected onto a 2D surface (the film) to form an image. Such images have no spatial resolution in the direction of the x-ray beam propagation resulting in the loss of depth information. For example, in a chest radiograph the lungs and ribs overlap (Swindell and Webb, 1988).

X-ray computed tomography is revolutionary in that it overcomes these limitations of the traditional radiograph. For instance, blood vessels and their actual location within a patient's anatomy may be viewed with x-ray CT by injecting the patient with a contrast medium.

2.3.2 The Basics of X-ray Computed Tomography

The basic principle underlying x-ray computed tomography (CT) is that internal structures of an object can be reconstructed by obtaining multiple projections of x-rays through the object. A projection is defined here as the x-ray intensity read by an array of detectors on the side of the imaged object opposite the x-ray source. The quality of the

image increases as the number of ray projections used to reconstruct the image increases. In modern CT scanners the number of projections is upwards of 1000 and computer algorithms are used to reconstruct the image (Curry *et al*, 1990).

CT scanners have been improving rapidly since their introduction and most modern clinical CT scanners are third or fourth generation designs. Third generation scanners, often termed rotate-rotate scanners, have a detector array opposite a fan beam x-ray source that rotate together 360 degrees around the patient. Fourth generation scanners have a fixed, 360 degree detector array and a fan beam x-ray source that rotates 360 degrees inside the detector ring around the patient. This is often termed a fixed-rotate scanner (Curry *et al*, 1990, Brooks, 1980b, Swindell and Webb, 1988).

The radiation sources in all modern CT scanners are rotating anode, x-ray tubes operating in a diagnostic energy range (~80 – 140 keV). These produce focal spots as small as 0.6 mm in some units and allow for multiple slices to be acquired in sequence due to efficient heat dissipation. Detectors are either scintillation crystals (all fixed-rotate type scanners) or xenon gas ionization chambers (most rotate-rotate type scanners). The x-ray beam is collimated both at the x-ray tube and the detectors. The collimation at the tube serves to determine the slice thickness and at the detectors serves to control scattered radiation (Curry *et al*, 1990). For a description of the CT scanner used for the experiments in this thesis see section 3.3.

There are several algorithms used in CT scanners to reconstruct an image from projection data. The original method was back projection, where the image is reconstructed by smearing the projected ray sums back across the lines of projection. This method is no longer used in commercial CT reconstruction algorithms. The iterative method, occasionally

used, reconstructs the image by 1) starting with assumed values for all pixels in the image, 2) producing ray sums from these pixel values, 3) comparing these ray sums and the measured ray sums, 4) improving the assumed pixel values and 5) repeating. The most commonly used methods in modern clinical CT scanners are analytical methods. One such method that is frequently employed is called filtered back projection. Filtered back projection applies a filter designed to have high frequency emphasis (such as a high frequency ramp filter) to the spectral Fourier transform of each of the image projections. The reconstruction is completed through performing a simple back projection on the filtered projections (Brooks, 1980a, Gordon and Herman, 1974).

To obtain a clinical image, a patient lies on a couch that is moved into the bore of the CT scanner. Two dimensional (2D) image slices through the body are obtained in a plane perpendicular to the axis of the scanner bore and coincident with the plane of source and detector array. As previously discussed, x-ray CT imaging has two principle advantages over traditional x-ray projections. First, due to the collection of projection data from angles 360° around the patient, CT images provide improved soft tissue contrast. Second, by defining a 2D image plane depth information is resolved in CT images.

2.3.3 CT Numbers

The output from a CT scanner is called CT numbers. They are related to the attenuation coefficients of the object imaged by the following expression:

$$\text{CT number} = K \times \frac{(\mu - \mu_w)}{\mu_w} \quad (2.16)$$

where μ and μ_w are the linear attenuation coefficients of the material imaged and of water, respectively, and K is a scaling constant usually taken as 1000. Although unitless, CT

numbers for $K = 1000$ are called Hounsfield units (H). Most CT scanners can give a range of CT numbers from -1000 H to $+4000$ H (Curry *et al*, 1990, McCollough and Zink, 1998). Given an attenuation coefficient of zero for air, air has a CT number of -1000 H, water a CT number of 0 H, and compact bone gives CT numbers around $+1000$ H. CT numbers obtained from patient scans are therefore most often found in the range of -1000 H to $+1000$ H.

The CT numbers for a single scan are collected in a matrix of 512×512 pixels. To view the matrix, each CT number is assigned an intensity or grayscale. In order to maximize grayscale contrast in the image, window level and window width are chosen. The window level determines the CT number where the grayscale is centered, and the window width determines how many CT numbers will be represented by the range of gray levels (Curry *et al*, 1990). This windowing allows for a particular region of interest to be represented with high grayscale or contrast resolution.

2.3.4 Density and CT Number

The Compton effect is the most prominent interaction between x-rays of CT scanner energies (<140 keV) and the low atomic number (Z) materials found in the body. Since the photon attenuation due to Compton interactions involves photons scattering off “free” electrons (see Figure 2.1), CT numbers depend on electron density. Based on equation 2.16, CT numbers can be expressed in terms of electron densities as follows:

$$\text{CT number} = 1000 \times \frac{(\rho_{ew}^s - R_\sigma)}{R_\sigma} \quad (2.17)$$

where ρ_{ew}^s is the ratio of the electron density of the sample compared to that of water and

R_σ is the ratio of the electron cross sections of water to that of the sample (Kron *et al*, 1993).

The physical density of a material is related to its electron density by the following simple expression:

$$\rho_e = N_e \times \rho \quad . \quad (2.18)$$

where ρ and ρ_e are the material's physical and electron densities respectively and N_e is the number of electrons per unit mass of the material (McCollough and Zink, 1998). It is apparent from this expression that a change in the physical density of a sample results in a change in the sample's electron density and hence CT numbers.

2.3.5 Noise and Physical Limitations

The spatial resolution and density contrast visible in CT images (contrast resolution) are affected by several interrelated factors. The following is a brief overview of these factors.

1) Photon Statistics

Fundamental limitations to both spatial and contrast resolution in CT images are derived from the statistical nature of x-ray production, photon interactions with matter and photon detection. First, the number of photons emitted from the x-ray tubes per unit time form a Poisson distribution about a mean. The chance that the counts per unit time will equal the mean increases with length of time counting. Second, given a particular energy and medium, there is a given probability that a photon will be transmitted to the detector. This probability is pre-determined, but it is only a probability. Finally, the counts read at the detector will depend on the detector efficiency. Combining these factors, the number of photons counted by the detector is a sample of the Poisson distribution (McCullough, 1980). Increasing the amount of photons transmitted reduces this statistical limitation. However, in

clinical imaging, increasing resolution by this means is limited by other concerns, such as patient exposure and motion artifacts (Curry, 1990).

2) Beam Hardening

For a polyenergetic beam the spectrum changes, becoming more energetic, as it passes through a medium due to preferential absorption of low energy photons. It follows that x-rays going through a medium from different directions will have traveled across different amounts and types of tissue and will therefore have different spectra and be attenuated differently at a certain point. Thus, it is difficult to assign a single attenuation coefficient to the material at a point. The most common solution is to approximate the beam as monoenergetic by using methods for finding a sum of monoenergetic beams that correspond to measured polyenergetic ones. However, the beam hardening effect remains and is observed as streaks across CT images.

3) Finite Source and Detector Size

A projection of data results from x-rays defining a line between a point source and point detector. For a finite source and finite detector size as in a CT scanner, this "line" is in fact a column of thickness defined by the size of the source and detector. As a result, CT numbers are calculated for small volumes rather than points. This obviously affects image spatial resolution, but also affects the calculation of CT numbers. A CT number calculated for a volume containing two different materials will be a false average weighted slightly in favor of the smaller attenuation coefficient. This weighting is due to logarithms present in the calculation method and is commonly referred to as the partial volume effect.

4) Motion

Since the attenuation coefficient is a function of position, (x,y) , it is affected by organ motion. To limit this physical problem the time required between projections is reduced and for some studies patients are asked to hold their breath during imaging.

5) Scatter

A problem associated with an array of detectors as opposed to a single detector is that, due to detectors positioned at various angles towards the source, more scattered radiation is detected. Collimation around detectors is used to reduce the amount of scattered radiation that reaches the detectors, but not all scattered radiation is removed from the beam and this imposes a physical limitation on both the spatial and contrast resolution attainable by a CT scanner (Curry *et al*, 1990, Swindell and Webb, 1993).

As illustrated, all the factors mentioned, except for patient motion, will limit the attainable spatial or contrast resolution in CT images of PAG gel. The importance of these limitations is the resulting limitations imposed on the dose resolution attainable for CT PAG gel dosimetry.

CHAPTER 3

MATERIALS AND METHODS

Introduced in this chapter are the materials and methods employed in this investigation. A general overview of the gel dosimetry technique is provided in section 3.1. The details of gel preparation and irradiation are given in section 3.2. A description of the CT scanner used for imaging experiments and a discussion of our imaging technique is presented in section 3.3. Finally, the techniques used to prepare the images for viewing and analysis are discussed in section 3.4.

3.1 General Gel Dosimetry Technique

The general steps involved in gel dosimetry techniques are illustrated in Figure 3.1. The gel dosimeter is first prepared according to a specific recipe. It is then placed at the isocenter (axis of rotation) of a LINAC in a manner that is similar to a patient set-up, and irradiated with a treatment providing the desired dose distribution. As discussed in section 2.2, radiation induces chemical change in the dosimeter that, to an extent, is proportional to the locally absorbed dose. Following irradiation, the dosimeter is imaged using an imaging modality. Through image processing techniques, dose information resulting from the radiation treatment is extracted from images of the gel. This dose information can then be used to verify the doses calculated by the treatment planning system and the location of the dose distribution with respect to the planned location.

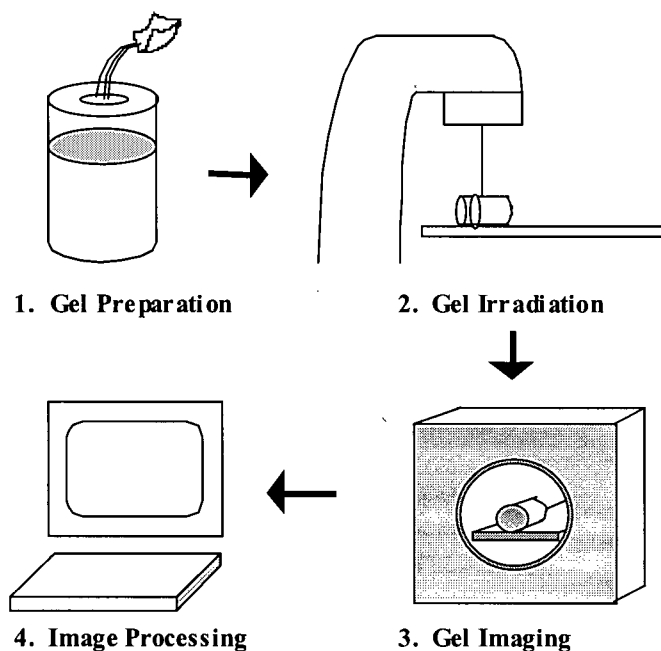


Figure 3.1 A general overview of the gel dosimetry technique.

3.2 Gel Preparation and Irradiation

The components of the PAG gel used for our experiments were acid-cured swine skin gelatin (300 bloom, Sigma Chem. Co., St. Louis, MO), electrophoresis grade acrylamide monomer, N,N'-methylene-bisacrylamide crosslinker (Bis) (both products of Sigma Chem. Co.) and triple distilled, de-ionized water. The composition (%weight) was: 5% gelatin; 3% Bis; 3% acrylamide and 89% water.

PAG gel was prepared as described by Audet, 1995. Water, gelatin and acrylamide were mixed into a container and heated in a microwave to 60°C. This warm solution was purged of oxygen by blowing nitrogen gas down the central funnel created by rapid stirring. The Bis was added once the mixture cooled to 40°C. Rapid stirring and deoxygenation continued for about an hour until all the Bis was dissolved. The gel was then capped, sealed

from light and refrigerated. It was ready for irradiation once it set. The gel used in this work had a final volume of approximately 1.5 L in a cylindrical container (diameter 12.7 cm, height 21 cm) made of 5 mm thick Perspex.

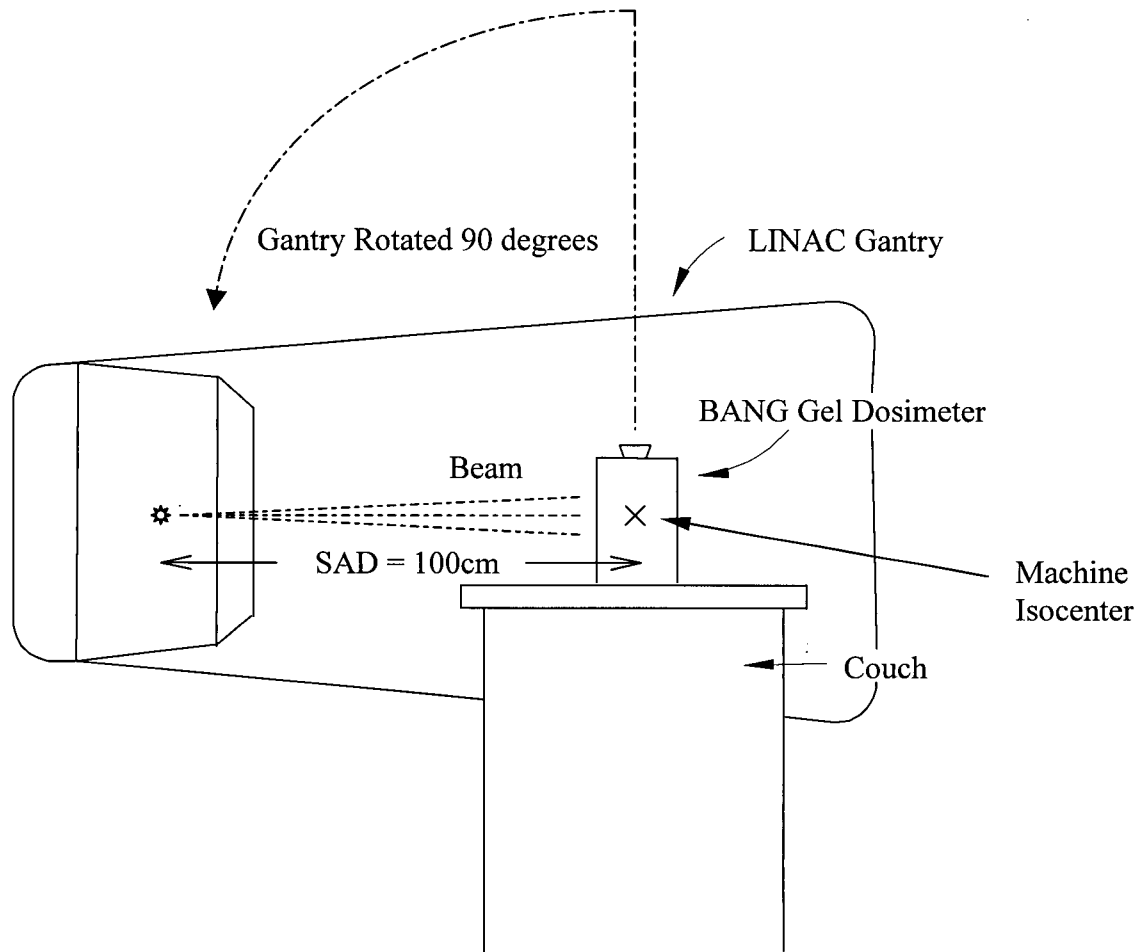


Figure 3.2 Set-up of our cylindrical PAG gel dosimeter for irradiation with a medical linear accelerator (LINAC).

Approximately 8 hours after preparation, the cylindrical PAG gel was irradiated using a 10 MV photon beam from a Varian Clinac 2100C linear accelerator (Varian Assoc., Palo Alto, CA). The set up, shown schematically in Figure 3.2, was in air, at a Source to Axis Distance (SAD) of 100 cm, with the LINAC gantry rotated to 90°. The gel was

irradiated (perpendicular to the cylinder wall) with four intersecting $3 \times 3 \text{ cm}^2$ beams, to doses of 2, 4, 6 and 8 Gy at the depth of maximum dose ($d_{\text{max}} \sim 2.5 \text{ cm}$ for 10 MV photons). This combination of beams is schematically illustrated in Figure 3.3. After waiting one day for the radiation induced co-polymerization to be completed, the gel was exposed to oxygen. Re-oxygenating the gel is important as it renders it inactive and therefore insensitive to further irradiation during CT scanning.

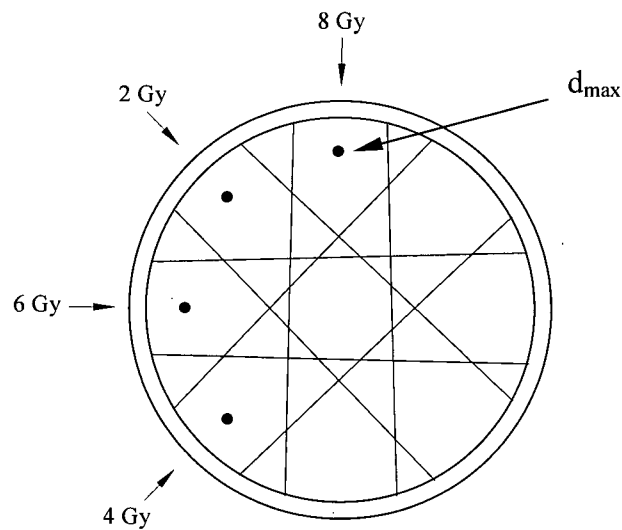


Figure 3.3 Top view schematic of the cylindrical PAG gel used in this investigation. The arrangement of the four intersecting $3 \times 3 \text{ cm}^2$ beams used in irradiation is illustrated. The depth of maximum dose (d_{max}) for 10MV photon beams, $\sim 2.5 \text{ cm}$, is illustrated by black dots.

3.3 CT Imaging Technique

CT imaging of the irradiated PAG gel was performed using a GE HiSpeed CT/*i*[®] CT scanner available in the Diagnostic Imaging Department of the Vancouver Cancer Centre. The scanner is a third generation, rotate-rotate scanner. This means an x-ray tube emitting a fan beam of radiation and an opposing array of scintillation detectors rotate simultaneously 360° around the patient. The detector array is coupled to a data acquisition system that

samples each detector cell at approximately 1000 times per second, amplifies and quantifies the current and sends the result to the image generator where a Fourier back projection algorithm reconstructs the image (HiSpeed CT/i[®] manual, 1997).

The cylindrical PAG gel, irradiated as described in section 3.2, was imaged in slices perpendicular to the cylindrical axis and through the center of the 3 x 3 cm² radiation beams. This is schematically illustrated in Figure 3.4. The gel was properly aligned in the scanner using perpendicular lasers available for alignment purposes. Reproducible positioning of the gel for scanning was achieved by placing the cylinder in a styrofoam cradle attached to the scanner table.

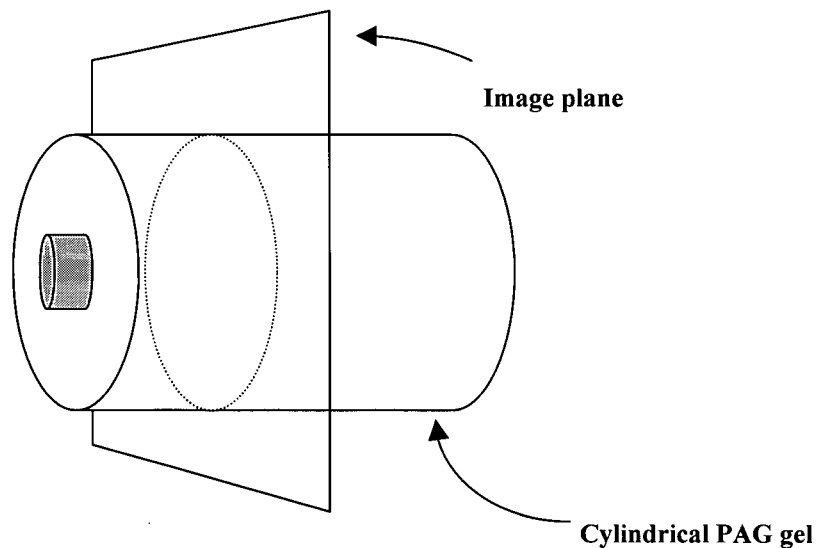


Figure 3.4 Schematic diagram illustrating orientation of PAG gel CT images perpendicular to the cylindrical axis of the gel.

There are many image acquisition parameters available on the CT scanner. The x-ray tube can operate at tube voltages of 80, 100, 120 and 140 kV and at tube currents ranging from 10 to 400 mA. Other parameter choices include: reconstruction algorithm mode (Normal, Detail, Edge or Bone); slice thickness; time per slice and field of view (FOV)

(HiSpeed CT/i[®] manual, 1997). These parameters were varied in an attempt to obtain the maximum sensitivity of image intensity to dose and high spatial resolution, while maintaining acceptable tube loading and imaging time. Table 3.1 lists all the CT parameters used for the imaging experiments. The resulting optimized CT imaging protocol developed from these imaging experiments is described in section 4.1. Images were also obtained at two gel temperatures, 4 and 23°C, to investigate the effect, if any, of gel temperature on the measured CT numbers. The optimized imaging protocol was used for all subsequent measurement of N_{CT} – dose responses (for example for the reproducibility studies in section 4.2.2).

Parameter	Setting
x-ray tube voltage	80,100,120 and 140 kV
x-ray tube current	100 - 300 and 400 mA
time/scan	1 s
FOV	25 x 25 cm ²
slice thickness	5 and 10 mm
Reconstruction Mode	Normal, Detail
Imaging Temperature	4 and 23 °C

Table 3.1 Parameter settings used for PAG gel CT imaging experiments on the GE HiSpeed CT/i[®] CT scanner.

3.4 Image Processing

Images obtained from the CT scanner are in a standard medical image format called DICOM (Digital Imaging and COmmunications in Medicine). They are 512x512 arrays of 2 byte binary numbers plus a header of variable length. Initial preparation of these DICOM images occurred on a UNIX workstation using a series of C programs written specifically for

processing CT images of PAG gel. The programs were used to perform the following tasks in sequence:

1. Convert the CT numbers delivered by the scanner to Hounsfield units
2. Change the image code from binary to ASCII
3. Zero the CT numbers in the region outside the gel phantom in order to increase image contrast in the useful image
4. Average anywhere from four to sixty-four image slices together if an increased signal to noise ratio is required.

Following these steps performed on the UNIX operating system, the images were transferred to a PC where they were viewed, further processed and analysed in the public domain NIH Image program (developed at the U.S. National Institutes of Health and available on the Internet at <http://rsb.info.nih.gov/nih-image/>). The NIH Image software was also used to filter images.

3.5 Dose Measurements

In order to construct N_{CT} – dose response curves for the PAG gel dosimeter, dose values had to be obtained for the same regions of interest in the PAG gel where CT numbers were extracted. The dose values for the PAG gel were calculated using XPlan, an in house treatment planning system available at the Vancouver Cancer Centre. A treatment plan was created for the four field irradiation performed on the PAG gel (see Figure 3.3) and used to determine the average dose in the regions of interest in the PAG gel. It has been verified previously that, for simple beam geometries and phantoms, XPlan provides accurate dose calculations.

3.6 Techniques for Determining PAG Gel Density

The fact that CT images of irradiated PAG gel show dose information implies that density changes are occurring in PAG gel in response to ionizing radiation. Three independent methods were used to determine the density of non-irradiated PAG gel. Calculating the density in several different ways supports the accuracy of the results and also provides options from which to determine the most accurate method of measuring PAG gel density. The three methods used were:

- 1) Mass and volume measurements
- 2) Calculations made directly from the N_{CT} measurements of the PAG gel
- 3) Construction of a N_{CT} – density calibration curve for our CT scanner to convert N_{CT} measurements to PAG gel density.

The first method was used to determine PAG gel density at room temperature only (23°C) and the last two methods were used at both 23 and 4°C.

Density Calculated by Mass and Volume Measurements

Using the same PAG gel composition as the gel employed in the studies presented earlier (see section 3.2 for the preparation technique), a PAG gel was prepared in a 100 mL graduated cylinder. The final solidified volume was 55.5 ± 0.5 ml. It was difficult to measure the gel volume due to a large meniscus formed at the gel's surface. The meniscus was the greatest source of uncertainty for density measurements made using this technique. Using an electronic balance, the mass of the graduated cylinder with and without the gel was measured. From these mass and volume measurements, the density of non-irradiated PAG gel was calculated.

Density Calculated from PAG Gel N_{CT} Measurements

From the measurement of a CT number, the physical density of the imaged material (sample) can be derived. Recall that, as described in section 2.3.4, CT number can be expressed as:

$$N_{CT} = 1000 \times \frac{(\rho_e^w - R_\sigma)}{R_\sigma} \quad (3.1)$$

In this expression, R_σ , the ratio of the water electronic cross section to the sample's (designated by subscripts and superscripts), is given by:

$$R_\sigma = \left[\sum f_i \left(\frac{\mu}{\rho} \right)_i \left(\frac{A}{Z} \right)_i \right]_{sample}^{water} \quad (3.2)$$

where μ/ρ , Z , A , and f_i are mass attenuation coefficient, atomic number, atomic mass and fraction by weight of element i , respectively, and the square brackets with sub and superscripts represents a ratio.

The relative electron density of the sample compared to water, ρ_e^w , as required in Equation 3.1, is determined from the expression:

$$\rho_e^w = \frac{N_A \rho}{\rho_{ew}} \left[\sum f_i \left(\frac{Z}{A} \right)_i \right] \quad (3.3)$$

where N_A is Avogadro's constant ($6.023 \times 10^{23} \text{ mol}^{-1}$), ρ is the physical density of the sample, ρ_{ew} is the electron density of water, and Z , A , and f_i are as given above. The electron density of water is given by the physical density of water at the imaging temperature multiplied by the number of electrons per gram in water, $3.343 \times 10^{23} \text{ e}^-/\text{g}$ (CRC Handbook, 1984). Given a CT number for non-irradiated PAG gel and using the results of Equations 3.3

and 3.2, the physical density of non-irradiated PAG gel is calculated from Equation 3.1. (For the details of this calculation, please see Appendix I).

It is important to note that in order to employ this method the energy of the photon beam delivered from the scanner x-ray tube must be known. This is because the photon energy determines the amount of attenuation in a material, and hence the mass attenuation coefficient (μ/ρ) in equation 3.2 (Johns and Cunningham, 1983). However, x-ray tubes do not deliver photons of a single energy, but a poly-energetic spectrum of bremsstrahlung photons. Thus, to determine the attenuation coefficients the multi-energetic beam must be approximated by the single energy that provides an attenuation that is as close as possible to that of the poly-energetic beam. This energy is called an effective energy (E_{eff}). At a 120 kV tube voltage setting the effective energy for a CT scanner is found to be 70.7 ± 1.0 keV by White *et al* (1980). Although this value will vary with x-ray tube variety and age, it will serve as a good approximation for the effective energy of our x-ray tube if it is operated at a tube voltage of 120kV.

Density Determined from an N_{CT} - Density Calibration Curve

By measuring N_{CT} for several materials of known density, a N_{CT} - density calibration curve was obtained for our CT scanner operating at the 120 kV tube voltage setting. The materials used were: Delrin ($\rho = 1540$ kg/m³), Perspex ($\rho = 1190$ kg/m³), Water ($\rho = 1000$ kg/m³) and Polyethylene ($\rho = 925$ kg/m³). Images of these materials were obtained during a single scan to avoid error due to changes in scanner tube temperature. Figure 3.5 shows the resulting calibration curve.

A linear regression performed on the calibration curve gave the following result with a correlation coefficient of 0.99994:

$$N_{CT} = (0.659 \pm 0.005) \rho_{gel} - (661 \pm 6) \text{ kg/m}^3 \quad (3.4)$$

Thus, the density can be determined from measured N_{CT} values by using the following linear relationship:

$$\rho_{gel} = (1.52 \pm 0.01) N_{CT} + (100 \pm 2) \times 10 \text{ kg/m}^3 \quad (3.5)$$

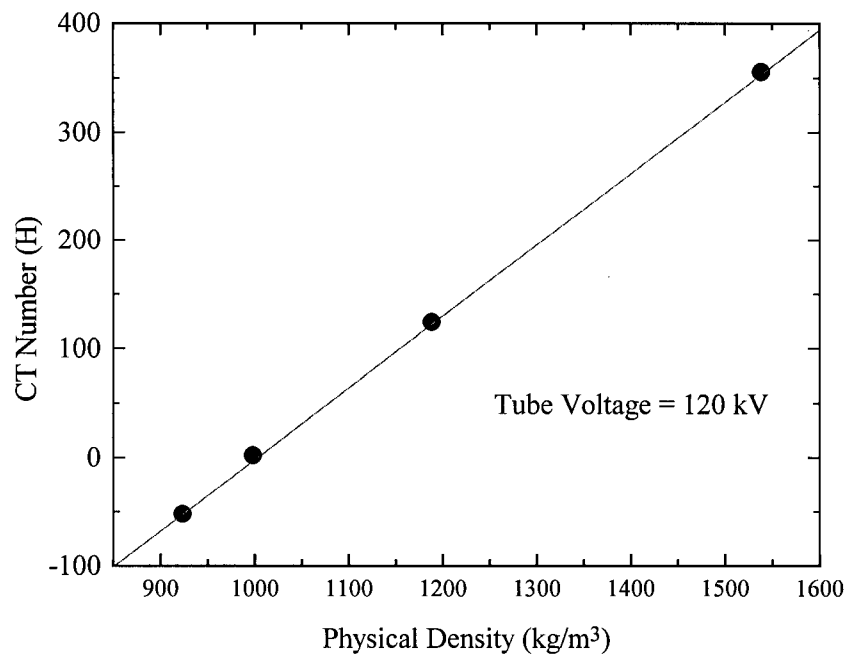


Figure 3.5 The relationship between measured N_{CT} and known density of various materials for the GE HiSpeed CT/i CT. All CT measurements were performed during a single scan with a tube voltage setting of 120 kV.

CHAPTER 4

RESULTS AND DISCUSSION

An image of a single slice CT scan through the irradiated region of the PAG gel dosimeter described in Section 3.3 is displayed in Figure 4.1. Although obscured by noise and artifacts, this preliminary result shows the star pattern dose distribution expected from irradiation with four intersecting beams. Hence, density changes are occurring in the PAG

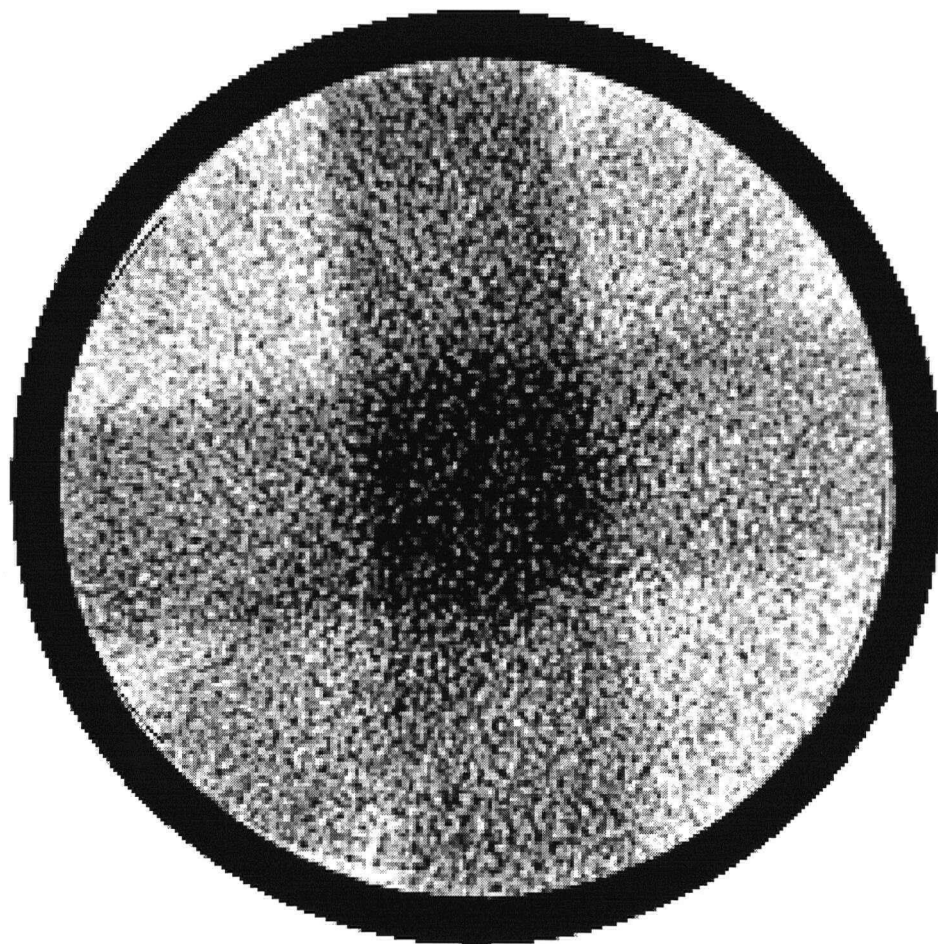


Figure 4.1 Preliminary CT scan across a PAG Gel irradiated, as described in Section 3.3, with four intersecting beams (2, 4, 6 and 8 Gy at d_{max}). Beneath the high noise the expected star pattern result is just visible in this image.

gel in response to absorbed radiation dose and CT images can be used to extract dose information from irradiated PAG gel.

The results of investigating the feasibility of a CT PAG gel dosimetry technique are presented and discussed in this chapter. Part of the investigation involved the development of an optimum CT imaging protocol used to maximize the quality of PAG gel CT images (section 4.1). With an optimum imaging protocol established, the N_{CT} – dose response of the CT PAG gel dosimeter was investigated. In section 4.2 is described the nature and reproducibility of this response. This is followed by a comparison of dose information derived using the CT and MRI PAG gel dosimetry technique and a discussion of advantages and disadvantages of the two techniques (section 4.3). Section 4.4 concludes this chapter with a brief quantitative assessment of the density change occurring in the PAG gel in response to ionizing radiation.

4.1 CT Imaging Protocol

Single scan images of our PAG gel, as illustrated in Figure 4.1, suffer from poor image quality. For this reason, a CT imaging protocol was developed to improve image quality before the potential for CT PAG gel dosimetry could be evaluated. In this section is presented an optimum CT imaging protocol and the rationale behind it. The optimization of CT imaging parameters to produce images with maximum contrast and resolution is discussed in section 4.1.1. In section 4.1.2, the problem of noise in the images obscuring dose information is addressed, and a method for increasing image signal to noise ratio is presented. Image artifacts also obscure dose information in the CT images. These artifacts

and a method of removing them from PAG gel images, are discussed in Section 4.1.3. In the final Section, 4.1.4, an optimum method for digitally filtering PAG gel CT images is discussed, and the results of this filtering are presented.

4.1.1 Optimum CT Imaging Parameters

There are many image acquisition parameters that may be varied when CT imaging. These parameters include: x-ray tube voltage and current, scan time, field of view and reconstruction mode (see Table 3.1 in Section 3.3). In an attempt to obtain a set of imaging parameters that produce high quality PAG gel images, the available parameter settings were systematically varied and the quality of the resulting images was analysed.

X-ray Tube Voltage

X-ray tube voltage (kV) is an important acquisition parameter that affects both the signal strength and the sensitivity of image intensity to changes in composition. The first point can be easily understood by recognizing that detected signal strength is proportional to the fraction of transmitted photons (I):

$$I = I_0 e^{-\mu x} \quad (4.1)$$

where I_0 is the initial number of photons produced by the x-ray tube, μ is the attenuation coefficient and x the thickness of the material. Both I_0 and I increase with tube voltage. The initial number of photons increases because the high tube voltage increases the number of electrons accelerated across the tube and hitting the anode target. The transmitted number of photons increases with increasing photon energy because the attenuation coefficient decreases with energy in this range. This decrease in the attenuation coefficient is a property of the photoelectric effect and Compton scattering interaction which are the dominant

interactions between photons and matter at diagnostic imaging energies (see Section 2.1.1). The final result is that a high tube voltage is preferred for maximizing signal strength.

The effect of kV on the sensitivity of the image intensity to changes in composition is more complex. Sensitivity in a CT image increases if the change in N_{CT} measured per change in object density increases. As stated above, attenuation coefficients which determine N_{CT} are a function of photon energy such that, in the < 140 keV range, attenuation coefficients increase as energy decreases. As a result, lower photon energies maximize the variation in attenuation coefficients between different materials and therefore image sensitivity (Johns and Cunningham, 1983). Since tube voltage determines the photon energy spectra leaving the x-ray tube, image sensitivity is expected to increase with decreasing tube voltage. Thus, signal strength and image sensitivity are affected in opposite ways by tube voltage, and a suitable compromise must be made.

Due to the small changes in density observed in the PAG gel, a low voltage setting was determined to be optimum in order to maximize image sensitivity and hence maximize sensitivity of the dosimeter. In order to investigate the variation in image sensitivity with tube voltage, N_{CT} was measured for materials of known densities at each tube voltage setting available on the scanner. The materials used had densities close to that of water to mimic the density changes in the tissue equivalent PAG gel.

Figure 4.2 consists of four graphs of N_{CT} as a function of density, one for each of the available x-ray tube voltage settings (80, 100, 120 and 140 kV). The densities investigated were those of Delrin ($\rho = 1540$ kg/m³), Perspex ($\rho = 1190$ kg/m³), Lexan ($\rho = 1170$ kg/m³) and Polyethylene ($\rho = 923$ kg/m³). By comparing the linear regression results from the

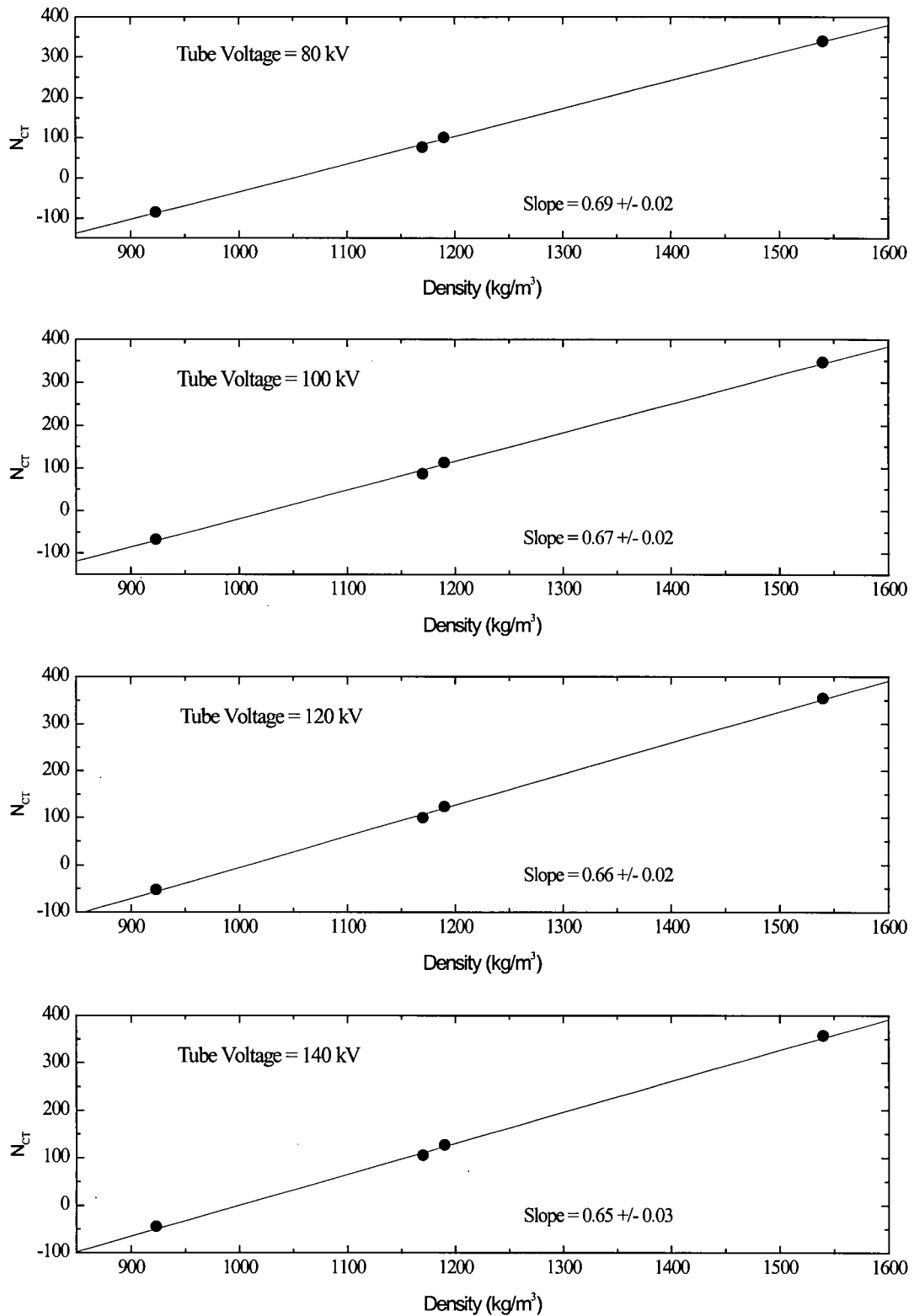


Figure 4.2 Sensitivity of N_{CT} to various densities near the density of water for all tube voltage (kV) setting available on the GE HiSpeed *CT/i*[®] CT scanner.

slopes of these four plots it is evident that, as expected, the sensitivity of N_{CT} to changes in density increases as the operating tube voltage decreases. Quantitatively, there is a 5% decrease in sensitivity between the 80 and 140kV tube voltage settings.

The range of N_{CT} values between the background (non-irradiated region) and the high dose region in CT images of the irradiated PAG gel is approximately 13 H. From the results illustrated in Figure 4.2, choice of tube voltage setting therefore provides a maximum variation of ~ 0.5 H to the N_{CT} range in the images. Based on this information it was determined that tube voltage setting does not significantly alter the sensitivity of the PAG gel images to small changes in density. The optimum voltage setting for imaging PAG gel was chosen to be 120 kV because this setting is most commonly used clinically and has the most regularly performed calibration procedures.

X-ray Tube Current

Choice of x-ray tube current is also important for CT image acquisition, particularly when images with low noise levels and high signal strength are required. In general, the noise in a CT image decreases and the signal strength increases with the number of photons reaching the detectors (I). The noise decreases because it results from Poisson statistical fluctuations in photons arriving at the detectors. Using Poisson statistics, the standard deviation in a measurement is defined by:

$$\text{standard deviation} = \sqrt{n} / n \quad (4.2)$$

where n is the number of photons detected (Curry *et al*, 1990, Webb 1993). The signal to noise ratio (SNR) is inversely proportional to this standard deviation. As illustrated previously, in Equation 4.1, the number of detected photons, and hence SNR, can be

increased by increasing the number of photons emitted from the x-ray tube (I_0). Since the x-ray tube current (mA) multiplied by scan time per slice (to give mAs) defines the number of photons emitted from the x-ray tube, it follows that, given a particular scan time per slice, increasing the current will increase the SNR in CT images.

In order to verify that increasing the tube current decreases the noise in PAG gel images, images were obtained using 100 and 200 mA tube current settings with 1s scan time. Shown in Figure 4.3 are the intensity profiles taken across the high dose region and extracted from images obtained with each of these current settings. (Note: Because noise levels are so high in single images, this point is best illustrated using images with reduced noise. Hence, the profiles shown in Figure 4.3 are from images with 64 slices averaged together. Please refer to the next section on SNR for an overview of image averaging results.) It is evident that noise is reduced in the second (200 mA) image compared to the first (100 mA) image. This confirms that image noise decreases with increasing tube current. Since the PAG gel images suffer from a poor SNR, they are best imaged using high tube currents.

The ability to increase SNR using tube current is limited by rapid heat loading of the x-ray tube. When many images must be scanned, heat loading can result in a waiting period between scans so that the x-ray tube can cool down enough to resume scanning. This not only increases the time required to complete the scanning session but, through continual operation at maximum tube temperature, puts undue stress on the x-ray tube. This is an issue associated with image averaging (refer to Section 4.1.2).

Another factor to consider when optimizing tube current is x-ray tube filament size. Filament size defines the focal spot dimensions on the x-ray tube anode. A small filament is

desired to maximize spatial resolution in the images. Operating our CT scanner with a tube voltage of 120 kV, the highest tube current that can be used with the small x-ray tube filament is 230 mA (GE HiSpeed CT/i[®] scanner user manual, 1997). Remaining below this limit, and compromising between x-ray tube head load and image SNR, 200 mA was chosen as the optimum current setting for imaging PAG gels on our CT scanner.

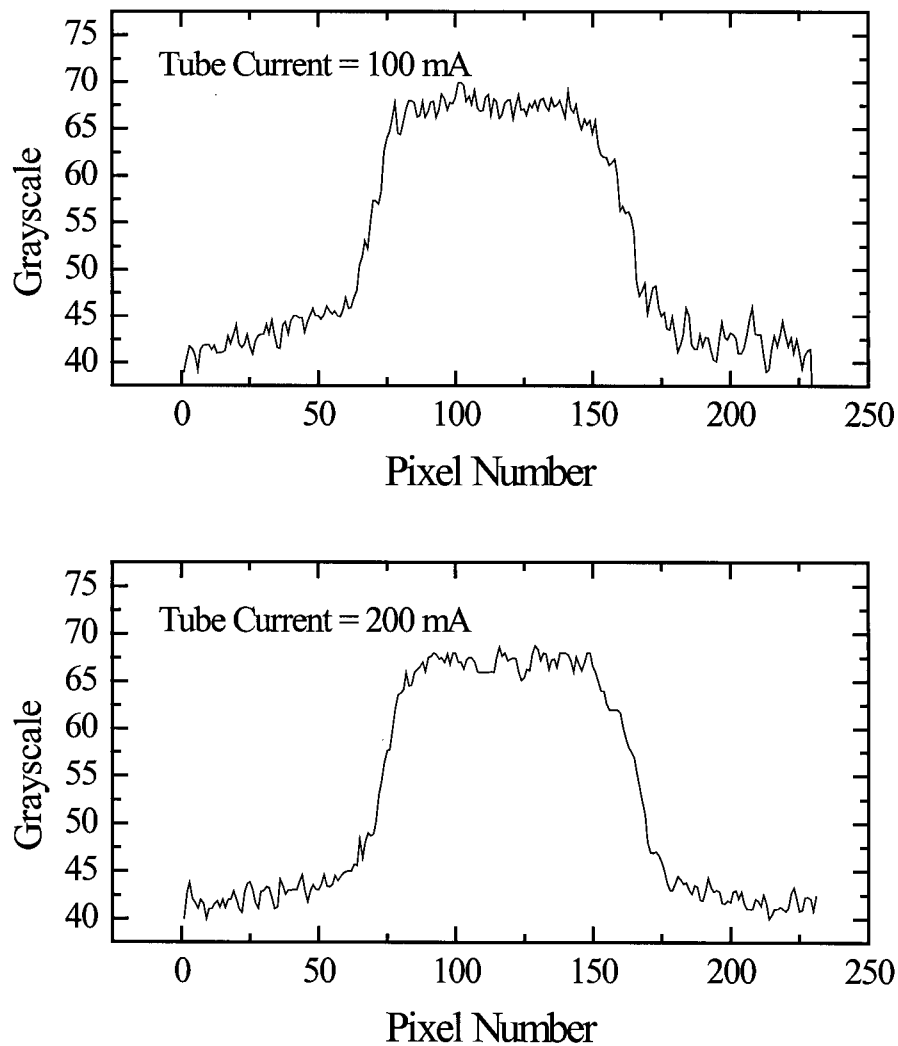


Figure 4.3 Image noise is reduced in CT images by increasing the operating tube current.

Other Image Acquisition Parameters

In addition to tube current and voltage, the settings for several other CT image acquisition parameters were optimized. Scan time per slice has briefly been mentioned above. As discussed, increasing scan time per slice increases mAs which increases image SNR. However, increasing scan time per slice will also increase image acquisition time. Thus, mAs and hence SNR, were maximized by operating at a high tube current rather than a high scan time per slice. In order to minimize image acquisition time, we chose to image with scan time per slice = 1 s.

The thickness of the CT slices is another parameter that has a range of possible values. The minimum slice thickness setting is 1 mm and the maximum is 10 mm. Optimizing this parameter involves a compromise between spatial resolution in the direction perpendicular to the image plane (z-direction) and image SNR. Slice thickness defines the spatial resolution in the z - direction in 2D images. When a 3D volume of CT images is considered, slice spacing also contributes to the spatial resolution in the z - direction. Increasing slice thickness decreases the spatial resolution in the z-direction through partial volume effects. On the other hand, SNR is proportional to the size of the volume element that defines an image pixel (a voxel). Thus, increasing slice thickness improves SNR (Sprawls, 1997). Because the SNR in the PAG gel images is so low (see Figure 4.1), optimizing SNR was preferred to optimizing spatial resolution in the z direction for this preliminary study. Also, since the PAG gel used in this study has a dose structure that remains relatively constant within the central 10 mm of the beams in the z direction, we do not obscure any dose information by collapsing 10 mm of z direction data into a 2D image.

For a discussion on improving SNR in PAG gel images of different slice thicknesses, see Section 4.1.2.

Other CT imaging parameters include reconstruction mode and field of view (FOV). The Detail reconstruction mode was chosen since this mode provides the best detail contrast in CT images (GE HiSpeed CT/i[®] scanner manual, 1997). The PAG gel was imaged using several of the available FOVs. The “Small” (25 x 25 cm²) FOV was preferred since it closely matched the size of a cross sectional image of our cylindrical gel and therefore provided the maximum spatial resolution in the image plane (x and y directions).

4.1.2 Signal to Noise Ratio and Image Averaging

As observed in Figure 4.1, poor image contrast due to noise is a problem in single PAG gel CT images. The signal to noise ratio (SNR) in these single images is 3.2, where SNR has been defined as:

$$\text{SNR} = \frac{\overline{N_{CT}}(\text{gel high dose region}) - \overline{N_{CT}}(\text{non - irradiated gel})}{\overline{N_{CT}}(\text{image noise})} \quad (4.3)$$

where $\overline{N_{CT}}$ denotes the average CT number from a small region of interest.

Factors affecting image SNR include image averaging and, as discussed previously, tube current, voltage and slice thickness. Image averaging increases SNR by effectively increasing the number of photons producing an image. It is important to note that this technique works only if the image noise and signal are uncorrelated. Since noise in CT images is random Poisson noise, image averaging is a good simple way of increasing SNR in CT images.

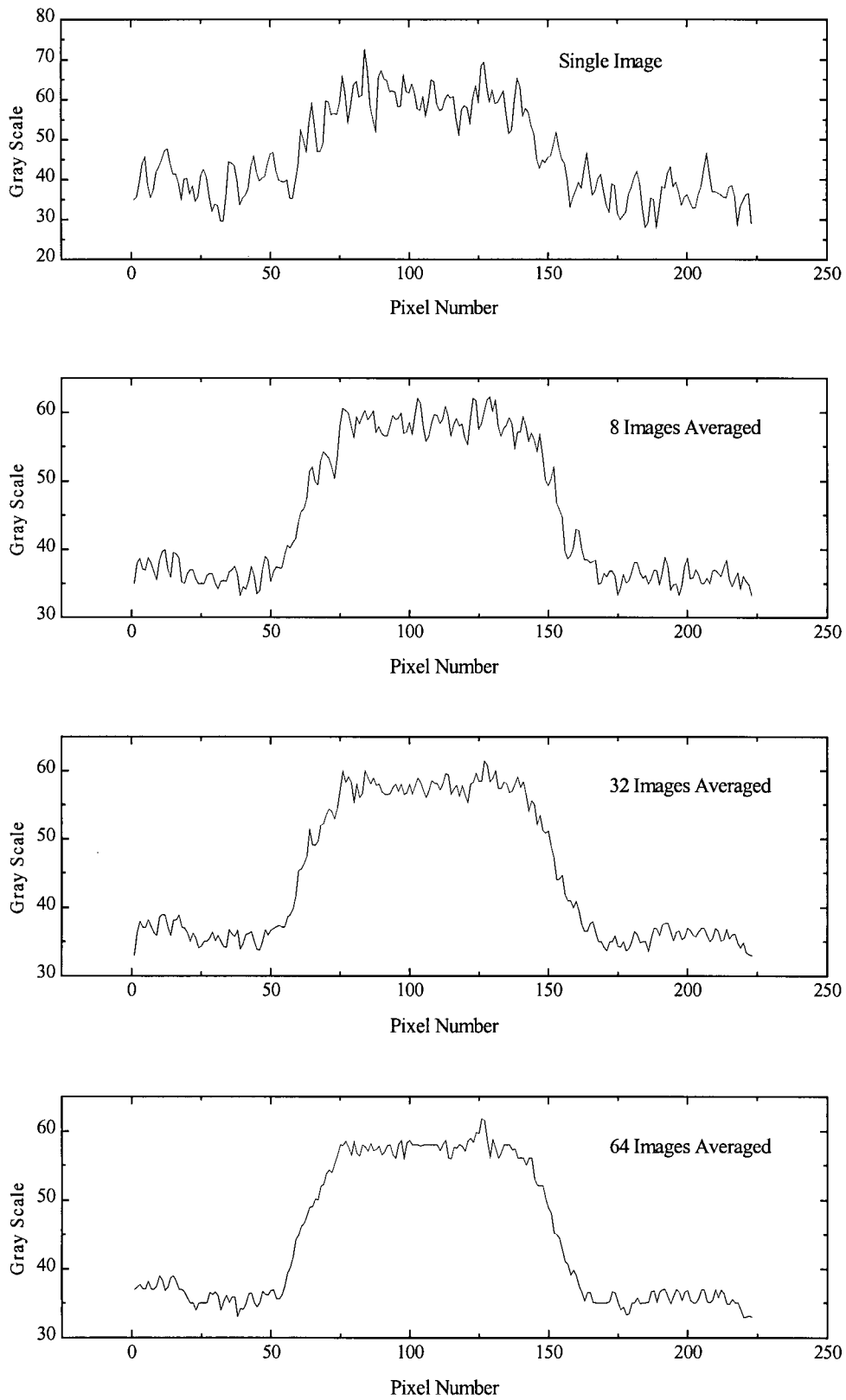


Figure 4.4 Intensity profiles indicating the reduction of image noise with image averaging.

To illustrate that image averaging does in fact reduce noise in PAG gel images, intensity profiles were obtained across the high dose region of images obtained by averaging various numbers of single images. Figure 4.4 compares these profiles for a non-averaged image and average images produced using 8, 32 and 64 images. The noise reduction obtained with image averaging is clearly visible.

As verification that slice thickness affects SNR, and to characterize how SNR increases with image averaging, SNR was measured for images derived by averaging 1 to 64 images and by using slice thicknesses of 10 mm and 5 mm. The results of these experiments are shown in Figure 4.5. Also shown is the \sqrt{N} theoretical increase in SNR with number of images averaged (N) (see Equation 4.2).

Several important observations can be made from Figure 4.5. As expected, SNR increases with N and slice thickness. Also, at low N , for both the 10 mm and 5 mm slice thicknesses, the increase in SNR with N approximately follows that predicted by theory. However, for higher N , SNR does not increase with N as predicted by theory. This deviation from theory occurs sooner for the 10 mm thick (dotted arrow) than the 5 mm thick (solid arrow) slice, and is most likely related to the limit in the N_{CT} resolution capable by the CT scanner. When the noise level reaches this limit, $\pm 1 N_{CT}$, noise reduction becomes more difficult and additional averaging produces only small changes in SNR. Since the images obtained with a 5 mm slice thickness are noisier than images obtained with a 10 mm slice thickness, it follows that the deviation of the measured SNR from the theoretical SNR occurs later for images of 5 mm than of 10 mm slice thickness. According to the results shown in Figure 4.5, the use of a 10 mm slice thickness maximizes the SNR of PAG gel images.

The optimum number of images used to produce an average image with improved SNR is a compromise between SNR and tube loading. If only a small number of slices through the dosimeter are required, 64 images per averaged image is recommended. This amount provides a good SNR (64 images averaged produces a noise level not much greater than ± 0.5 CT numbers) and yet avoids excessive x-ray tube heating that results from operating the CT scanner over many sequential scans. Averaging more than 64 images would produce great heat load and, based on the results observed in Figure 4.5, provide little increase in SNR. However, if many slices through the dosimeter are required, such as when

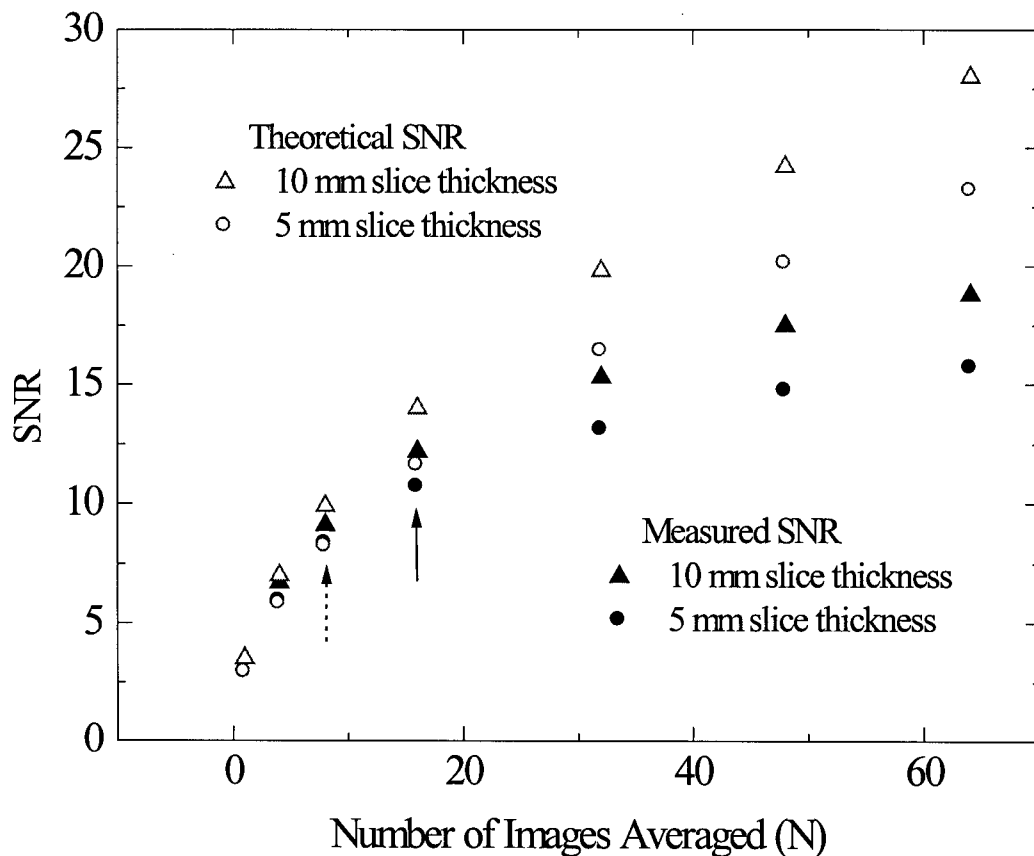


Figure 4.5 Increase in SNR obtained from N averaged images of our PAG gel compared with the \sqrt{N} increase expected from theory. SNR measurements are also compared for images with slice thicknesses of 10 and 5 mm.

producing a large 3D dose distribution, 16 or 32 images averaged per slice is recommended. The increase in SNR acquired by increasing the images averaged from 16 or 32 to 64 is too small to justify doubling the imaging time and increasing the stress on the scanner when acquiring large numbers of slices.

4.1.3 Artifacts

The success of image averaging in reducing the noise level in the PAG gel images (see Figure 4.1) is evident in the image displayed in Figure 4.6. This image was obtained using the optimum parameter settings listed in Table 4.1 (see Section 4.1.5) and averaging 64 images. However, even with improved SNR, useful dose information in the gel image is obscured by characteristic ring and beam hardening artifacts. The ring artifacts consist of rings concentric with the center of the CT scanner bore and the beam hardening artifacts are streaks across the gel image. Because the magnitudes of these artifacts are comparable to the useful dose information in the irradiated gel, the artifacts create a significant barrier to the extraction of accurate dose information from the gel.

The beam hardening artifacts result from the container wall being of higher density than the gel inside the container. Since lower energy x-rays are preferentially absorbed (see Section 2.1.1), a poly-energetic beam such as that delivered by the x-ray tube will get more energetic or "harder" as it passes through an attenuating media. This is called beam hardening and it causes the total beam attenuation to vary non-linearly with distance according to the materials traversed by the beam (Brooks, 1980). The visual effect on a CT image is that dark streaks or shadowing appear around high density structures as photons pass

from high to low density materials. These streaks are observed in the PAG gel image in Figure 4.6.

The observed ring artifacts are due to faulty or mis-calibrated detectors in the scanner (Curry *et al* 1990, Brooks 1980, Webb 1993). This is a characteristic artifact of images from third generation, rotate-rotate CT scanners such as the GE HiSpeed CT/i[®]. One can imagine that if a detector was faulty, as it rotated about the gel, a ring of incorrect data would appear in the image. In fourth generation rotate-fixed CT scanners where the detectors form a solid

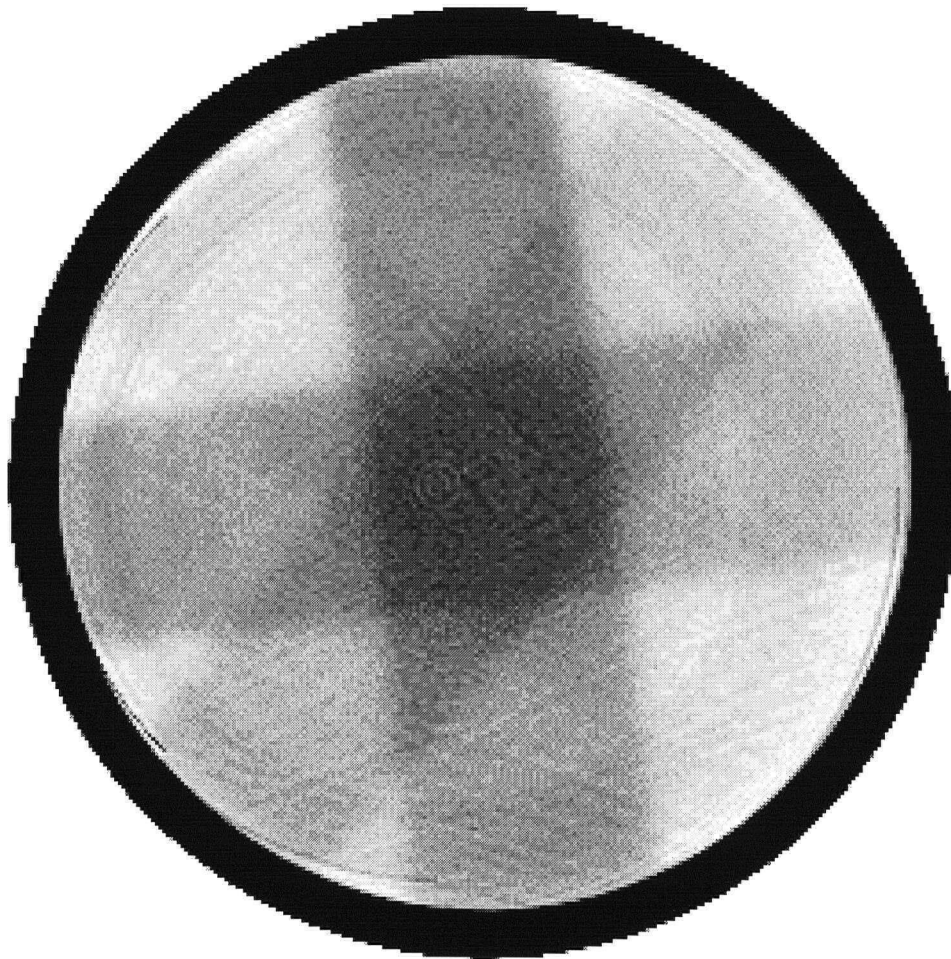


Figure 4.6 Noise reduced PAG gel CT image showing ring and beam hardening artifacts that obscure dose information. This image was produced using optimum imaging parameters and averaging 64 images.

ring, these rings artifacts have virtually been removed. For scanners where ring artifacts are possible, the rings are usually removed by periodic calibration of the scanner detectors using uniform density calibration phantoms. However, the magnitudes of the rings as shown in Figure 4.6 are too small to be significant in the normal diagnostic imaging use of the CT scanner and as a result are not removed by normal quality assurance procedures.

In order to remove both types of artifacts from the PAG-gel images, a background subtraction technique was employed. This involved imaging a non-irradiated PAG gel in addition to the irradiated gel during each imaging session and subtracting the blank image

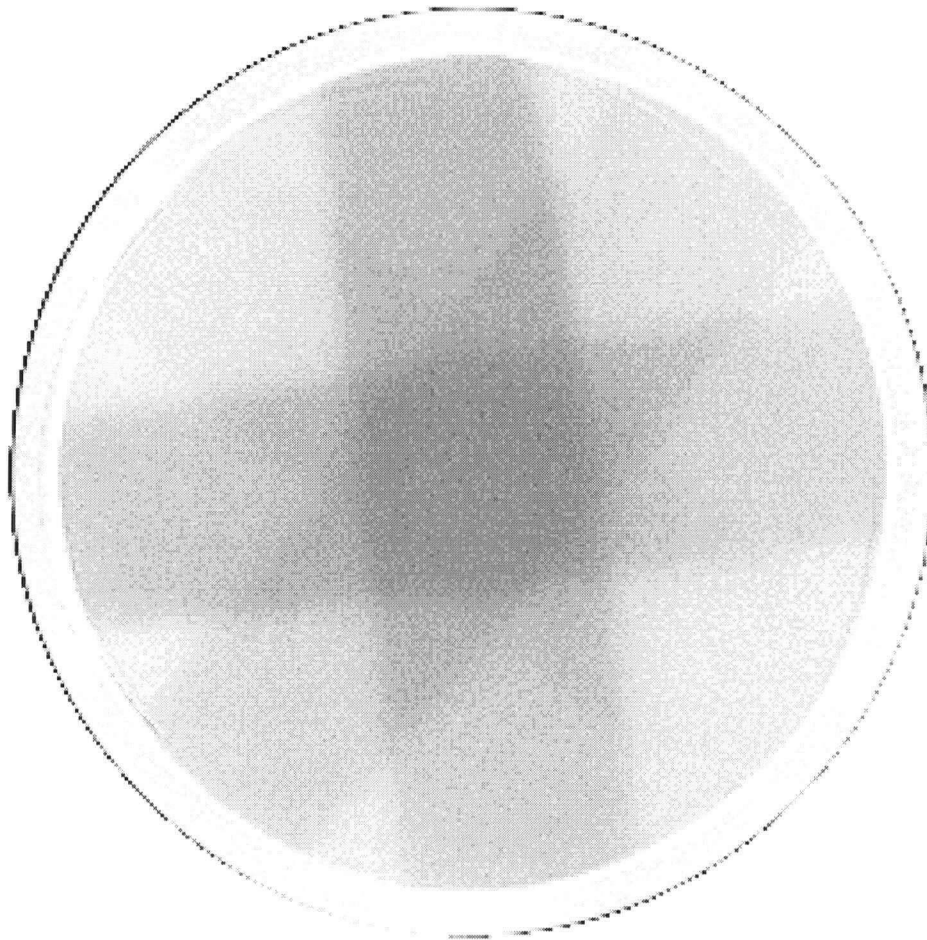


Figure 4.7 Final processed PAG gel CT image showing clearly the star pattern dose distribution resulting from a four field irradiation.

from the image of the irradiated PAG gel. It was important to position the blank and irradiated gel identically within the scanner bore to ensure identical rings in the images. The image subtraction was performed using the NIH image software. The success of this background subtraction technique in removing both types of artifacts is illustrated in Figure 4.7. Clearly evident is the star pattern dose distribution expected from the four field irradiation. Using the final CT imaging protocol of optimized imaging parameters, image averaging and background subtraction, quality PAG gel CT images that expose useful dose information have been produced. It is important to note that performing this background subtraction removes the true CT numbers associated with different densities in the gel. In order to retain true CT numbers for the density studies, the average background value was added to the subtracted image.

4.1.4 Digital Image Filtering

Once a method to produce quality images (see Figure 4.7) was developed, the use of digital image filters to further reduce noise in the images was investigated. The most well known type of digital smoothing filter is an averaging filter. This filter replaces each image pixel gray level with the average gray level in a 2D pixel array (called a mask) around that pixel. The mask dimensions can be adjusted by the user to maximize noise reduction while minimizing the smoothing out of fine structure in the image. Although successful in reducing image noise, this type of digital filter will always average out a certain amount of the sharp edges in an image (regardless of mask dimension). The results is a blurred image (Pratt, 1992).

Since accurate localization of high dose regions is of prime importance for the CT PAG gel dosimetry technique, edge reduction is not acceptable and a smoothing filter cannot be used to reduce image noise. An alternative approach to noise reduction is a median filter. This is a type of rank filter that operates like a smoothing filter except that each pixel is replaced by the median of the gray levels in the mask. The advantage a median filter provides is that, while removing impulsive noise, edges in an image are preserved (Pratt, 1992).

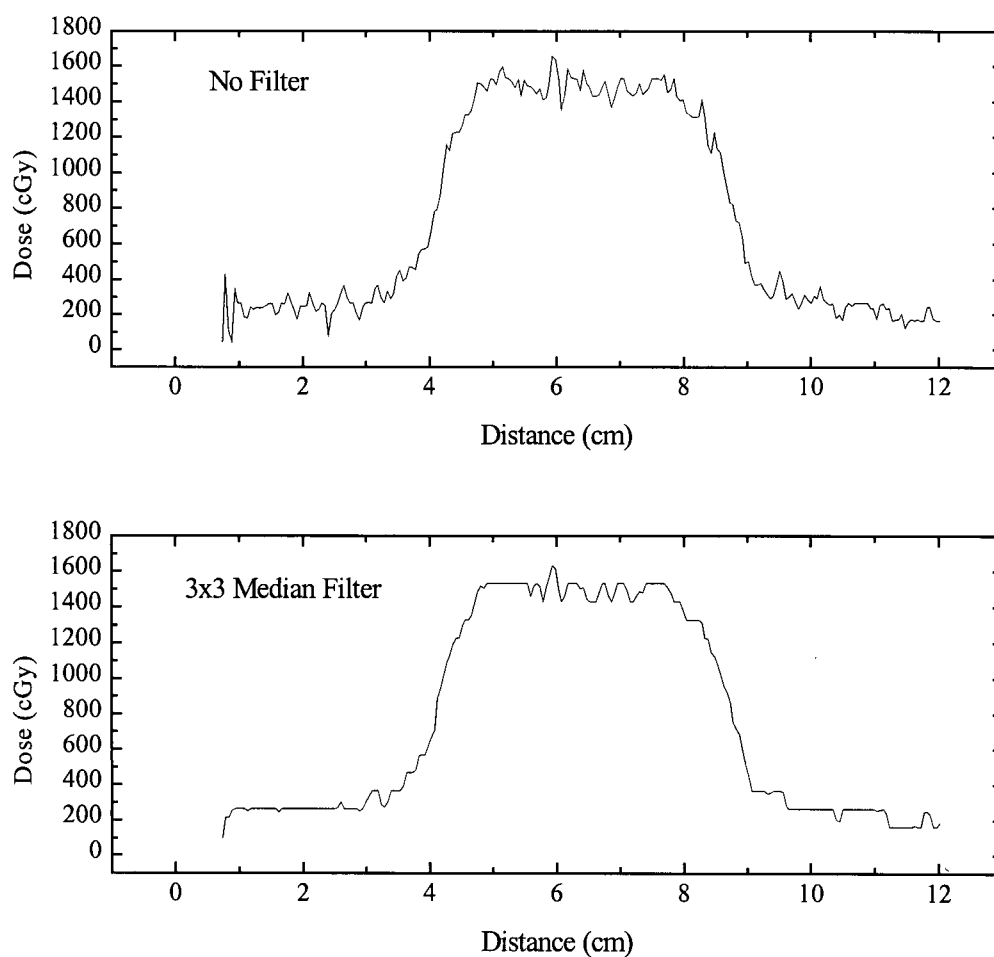


Figure 4.8 Effect of digital filtering a PAG gel CT image using a 3x3 median filter. Noise is reduced without compromising accurate localization of the high dose region.

Figure 4.8 shows a comparison between profiles taken across the high dose region of a 3 x 3 median filtered and a non-filtered gel image. The filtering was performed using NIH image software. The noise is reduced in the profile from the filtered image and importantly, the localization of the high dose region is preserved. Thus, median filtering is a good method for further reducing noise in PAG gel images.

4.1.5 Summary of CT Imaging Protocol

Table 4.1 summarizes all the parameter settings determined to be optimum for CT imaging PAG gel with the GE HiSpeed CT/i[®] scanner. The CT imaging protocol established in this study uses these parameters, averages 64 images (unless imaging a large 3D volume, then 16 or 32 images are averaged) and applies a background subtraction. The images can also be median filtered without compromising the spatial resolution of high dose regions, but filtering is not included in the CT imaging protocol employed in the studies that follow.

CT Imaging Parameter	Optimum Setting
X-ray Tube Voltage	120 kV
X-ray Tube Current	200 mA
Time/Scan	1 s
Field of View	small (25 cm x 25 cm)
Slice Thickness	10 mm
Reconstruction Mode	Detail

Table 4.1 Optimum parameter settings for imaging PAG gels with a GE HiSpeed CT/i[®] CT scanner.

4.2 CT Number – Dose Response

With an optimum CT imaging protocol available, the next step was to characterize the N_{CT} - dose response of the PAG gel (Section 4.2.1) and the reproducibility of this response (Section 4.2.2). The effect of gel temperature during imaging on the dose response was also investigated (Section 4.2.3).

4.2.1 Characterization of the N_{CT} – Dose Response

The relationship between N_{CT} and dose was determined by comparing, for several small, well defined regions of interest in the gel, the N_{CT} obtained from CT images of the PAG gel and absorbed dose calculated by a treatment planning system. Beam entrances and exits and the center of the high dose region were chosen as the regions of interest because they are easy to define reproducibly. Note that the error in CT number is +/- 0.5 H for all data points (not illustrated in the Figures that follow) and represents the standard deviations of the data values within the regions of interest.

Figure 4.9 illustrates the behavior of N_{CT} as a function of calculated absorbed dose. Many preliminary observations can be made from this graph. First, N_{CT} increases with dose. Since the amount of polymer produced is proportional to absorbed dose (Audet, 1995), and N_{CT} is proportional to density, it follows that gel density increases with polymerization. It is not intuitively obvious that this should be the case. Possible explanations for the density increase are 1) that the hydrophobicity of the polymer causes water to exude from the polymerized regions, or 2), that polymer is a condensed structure that doesn't contain water (Audet, 1998). Since water is probably less dense than strongly cross-linked polyacrylamide, the density of polymerized regions should be greater.

Qualitatively, the relationship between N_{CT} and dose is linear at doses below 8 Gy and then deviates from linearity at higher doses (see Figure 4.9). This general observation agrees with previously observed nuclear magnetic resonance (NMR) dose responses for PAG gels (Maryanski, *et al* 1993). An explanation has been proposed for the linear increase in the amount of cross-linked polyacrylamide with dose, and it is based on the propagation and termination of polymerization reactions (refer to Section 2.2.2) and the diffusion of reactions (Audet, 1995). It is interesting that the response after 8 Gy does not flatten out nearly as much as the previously observed R_2 -dose responses (Maryanski *et al*, 1994) and the saturation dose is not as well defined.

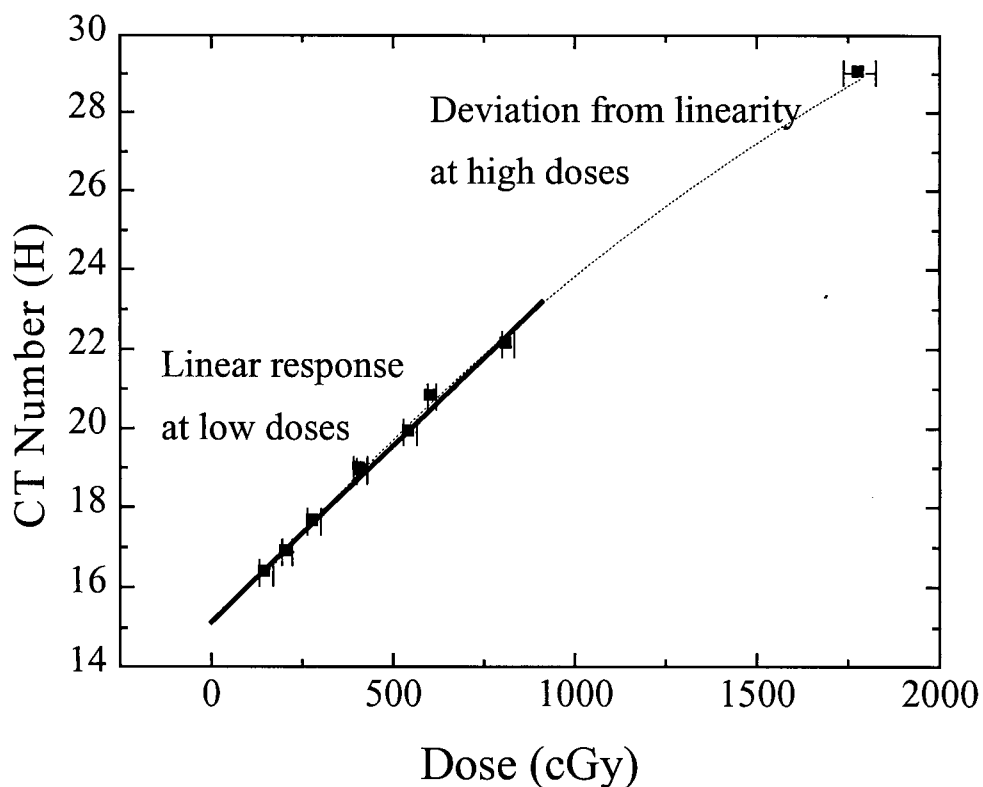


Figure 4.9 The N_{CT} – dose response of a PAG gel dosimeter. The dosimeter temperature was 23°C and the CT imaging protocol was employed (refer to Section 4.1.5). N_{CT} increases linearly with dose up to a point and then increases more slowly as higher doses are reached. Error bars represent the standard deviation in the average dose measured in regions of interest. Error in N_{CT} , not illustrated, is ± 0.5 H for all data points.

4.2.2 Reproducibility of the N_{CT} – Dose Response

The reproducibility of a linear N_{CT} – dose response (as observed in Figure 4.9 for doses < 8Gy) is all that is necessary for making relative dose measurements (refer to Section 2.1.3). However, establishing the reproducibility of the slope of the N_{CT} – dose response is necessary if CT imaging PAG gel can provide actual dose measurements. Ideally, for making actual dose measurements, a calibration curve would be reproducible over several imaging sessions, but at the very least it should be reproducible during a single imaging session. It is important to note that this feasibility study is solely concerned with the reproducibility of the dose response from a single PAG gel and that the issue of reproducibility of the dose response for different batches of PAG gel is not addressed.

Since making relative dose measurements requires a linear response, the studies that follow focus on the linear region (< 8Gy) of the PAG gel's N_{CT} - dose response (refer to Figure 4.9). It is important to note that for making actual dose measurements there is the potential for using the entire curve (up to 18Gy) in order to maximize SNR. To establish reproducibility of the linear N_{CT} - dose response, the response was measured for CT images obtained with the gel situated in different parts of the scanner, for images obtained in sequence during a single scanning session and for images obtained over different scanning days. All the images used in the reproducibility studies were obtained using the CT imaging protocol (refer to Section 4.1.5)

Reproducibility for Different Positions in the Scanner

When placing the gel in different parts of the CT scanner, significant variation in N_{CT} measured at particular regions in the gel was noted. It was determined that this variation in N_{CT} resulted from variable positioning of the ring artifacts present in the images. Since the rings are always concentric with the scanner bore, it follows that varying the gel position in the scanner would vary the position of the rings with respect to the gel's dose information. However, with the implementation of background subtraction to remove the rings, the reproducibility of the N_{CT} -dose response was improved and the responses agreed within error limits. This reproducibility is apparent in Figure 4.10 which shows the N_{CT} -dose

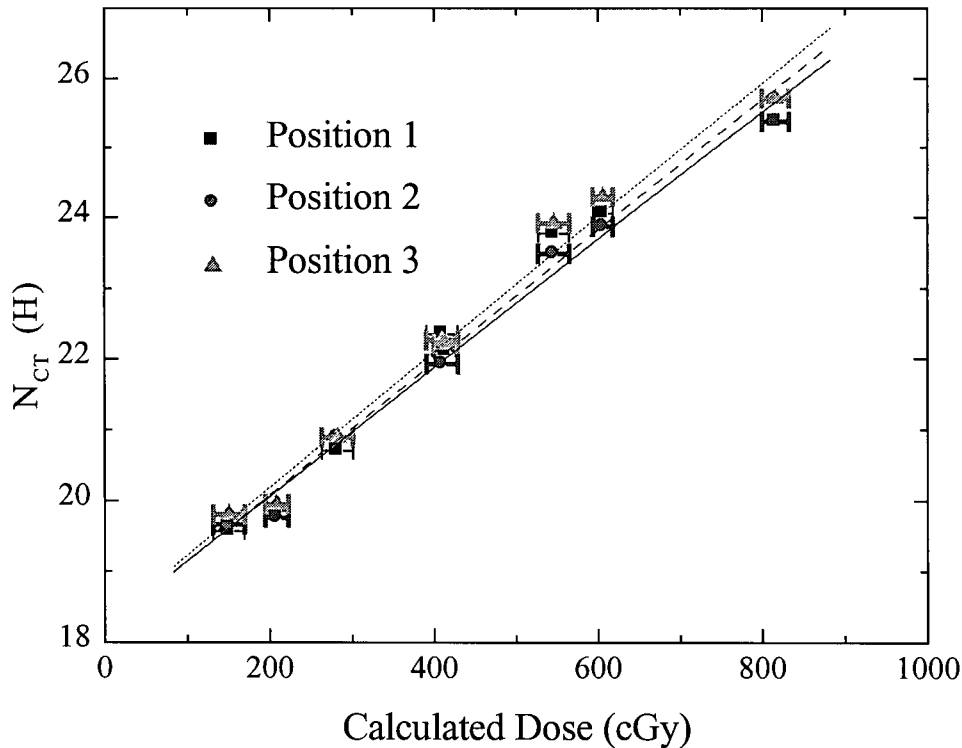


Figure 4.10 The PAG gel's N_{CT} -dose response for images obtained with the gel at different positions in the CT scanner. For all images, the CT imaging protocol was employed (refer to Section 4.1.5). Error bars represent the standard deviation in the average dose measured in regions of interest. Error in N_{CT} , not illustrated, is $\pm 0.5 N_{CT}$ for all data points.

responses at three different scanner positions. The slight variations in the responses are likely due to a factor other than gel position in the scanner that is discussed in the following section.

Reproducibility During a Single Scanning Session

The reproducibility of the N_{CT} - dose response was investigated for images obtained during a single imaging session and with the gel always positioned at the same location in the CT scanner (see Figure 4.11). The linear regression results indicate that the slope or dose sensitivity of this N_{CT} - dose response is the same for all images obtained during a single imaging session and is given by:

$$\Delta N_{CT} (H) / \Delta \text{Dose} (cGy) = (8.6 \pm 0.4) \times 10^{-3} \text{ H/cGy} \quad (4.5)$$

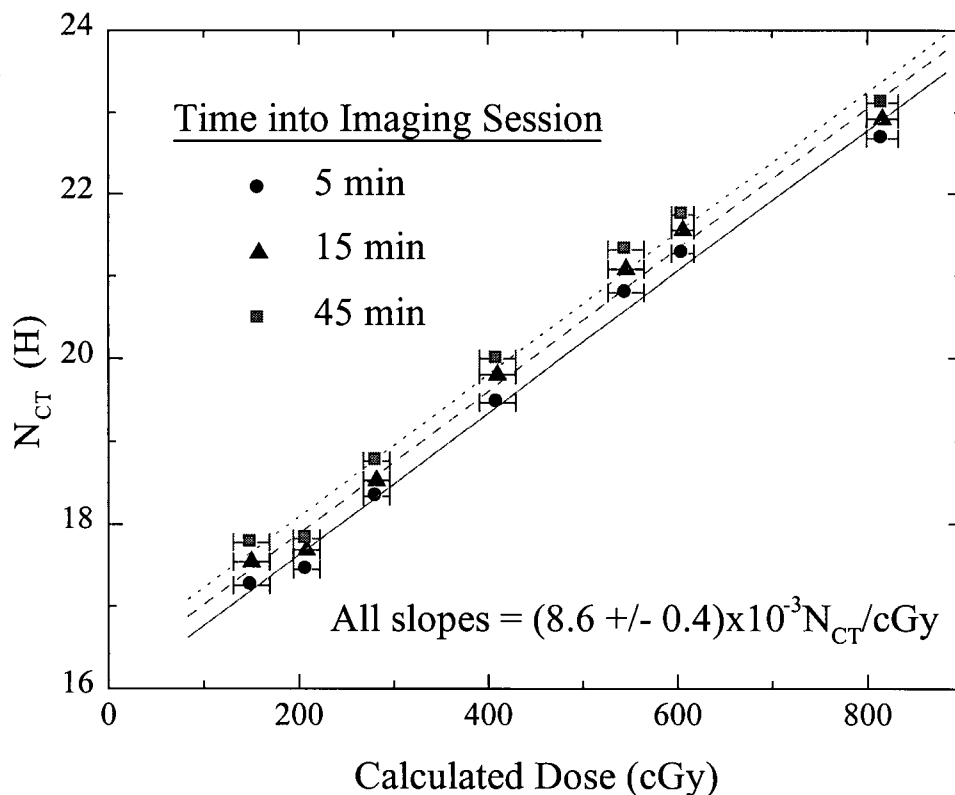


Figure 4.11 N_{CT} - response curves obtained for the PAG gel dosimeter during a single imaging session. The dosimeter temperature was 23°C and the CT imaging protocol was employed (refer to Section 4.1.5). Error bars represent the standard deviation in the average dose measured in regions of interest. The error in N_{CT} is only $\pm 0.5 N_{CT}$ for all data points and therefore is not illustrated.

However, a small upward shift in the N_{CT} - dose response was observed over time. This shift was measured consistently during every imaging session and was also observed, but not explained, in a study by Fallone *et al* (1982). The shift is most likely the result of x-ray tube heating during continuous imaging. Figure 4.12 shows the shift in grayscale values detected over time for three different locations in the PAG gel. The observed shift is consistent in all the plots and shows the grayscale values leveling off after about 45 min of scanner operation. This behaviour follows that expected from the tube heating since the tube temperature increases with operating time until it saturates at a maximum operating temperature. X-ray tube temperature is likely the source of variation the in N_{CT} - dose response shown in Figure 4.10 as well.

The magnitude of the shift in the N_{CT} - dose response with imaging time is < 1 H over the full operating temperature range of the scanner (see Figure 4.11) and therefore falls within the ± 0.5 H uncertainty in N_{CT} . The fact that the N_{CT} - dose response remains linear over time during an imaging session, regardless of shift, implies that the CT PAG gel dosimetry technique can be used for making relative dose measurements (see Section 2.1.3). The fact that the slope of the response remains relatively constant during a whole imaging session and that the shift is minimal, implies that the response may be used as a calibration curve to provide actual dose measurements from PAG gel images.

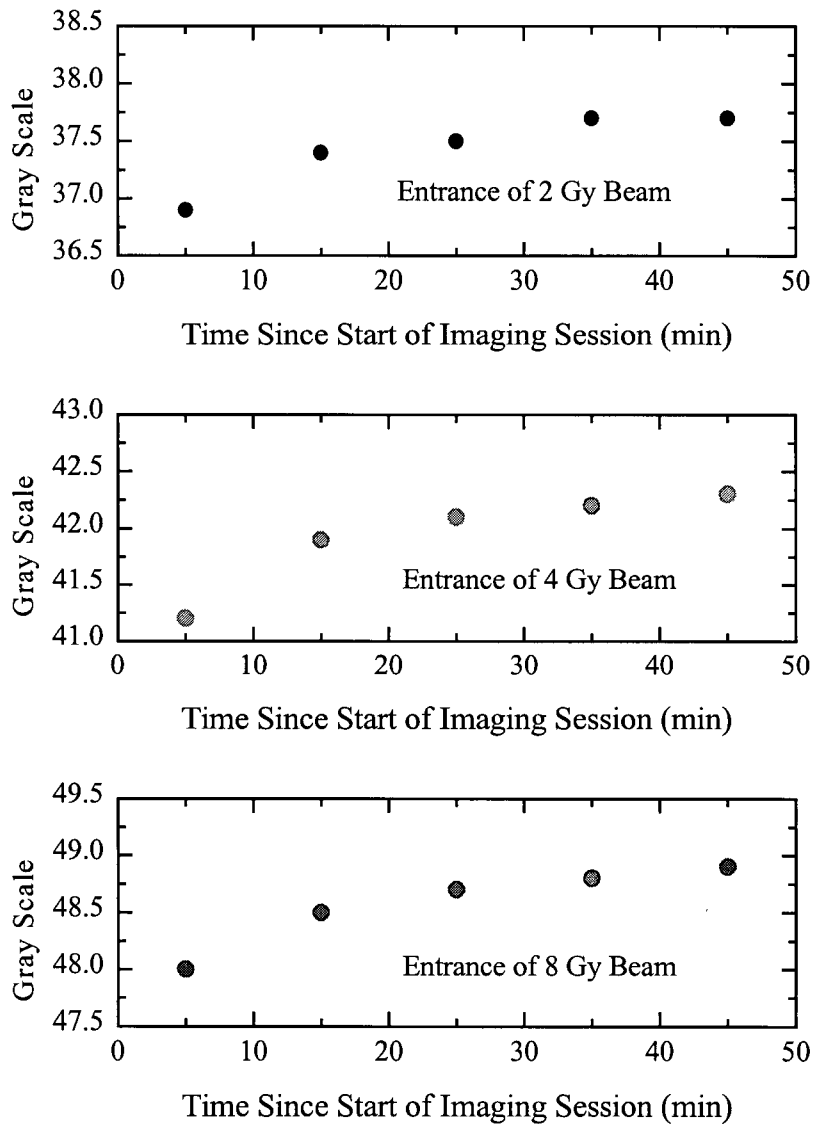


Figure 4.12 Shift in image intensity or grayscale measured over time into imaging the session for different regions in the PAG gel.

Reproducibility Over Different Imaging Sessions

The reproducibility of the relationship between N_{CT} and absorbed dose was also investigated for images obtained on different days. Figure 4.13 displays encouraging results from CT images obtained on three different days. It demonstrates that the N_{CT} -dose response (up to 800 or 1000 cGy) remains linear over several imaging days and therefore the

CT PAG gel technique can be provide relative dose measurements on any day. Not only is the linearity reproduced over several months, but so are the actual slopes (or dose sensitivities) of the N_{CT} -dose responses. This is a very promising result in that it implies that a single calibration curve can be used to obtain dose information from a PAG gel. However, the precision of the results would probably be improved by taking a baseline calibration at the start of each imaging session since this would account for the slight shifts in response as well as any unforeseen changes in the CT scanner. The shifts in the response observed in Figure 4.13 are arbitrary and cannot be characterized for the particular scanner used in this study. (It should be noted that this shift may not be observed for other scanners or types of scanners).

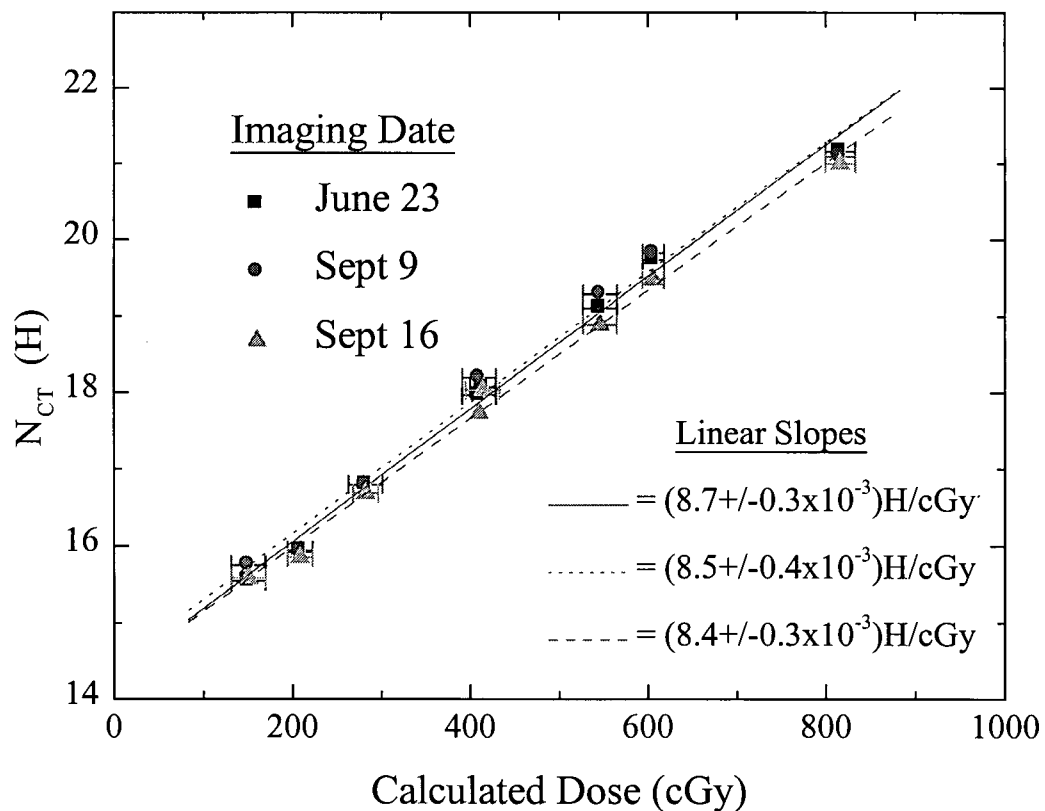


Figure 4.13 N_{CT} - dose response curves obtained for our four field PAG gel dosimeter over a series of several imaging sessions. The dosimeter was at 23°C, and the CT imaging protocol was employed (refer to Section 4.1.5). Error bars represent the standard deviation in the average dose measured in regions of interest. Error in N_{CT} , not illustrated, is $\pm 0.5 N_{CT}$ for all data points.

Dose Resolution and Minimum Detectable Dose

The dose resolution for actual dose measurements made using the CT PAG gel dosimetry technique, is derived from the uncertainties in ΔN_{CT} and in the sensitivity of the N_{CT} -dose response, using Equation 2.11 (see Section 2.1.3). Using the minimum detectable ΔN_{CT} (1 H) in Equation 2.11, the dose resolution for actual dose measurements is determined to be 60 cGy. Realistically, in order to be detected above background, the minimum detectable dose should be at least two times the dose resolution, or 120 cGy.

The dose resolution for relative dose measurements obtained using the linear N_{CT} -dose response, is given by Equation 2.9 (see Section 2.1.3). For example, the relative measure of a dose with $N_{CT} = 18$ H to the maximum linear dose ($N_{CT} = 23$ H) has an associated uncertainty of 4%. This uncertainty is a measure of the dose resolution for relative dose measurements. It is apparent that, for the CT PAG gel dosimetry technique, the dose resolution is greater for relative than for actual dose measurements.

4.2.3 Effect of PAG Gel Imaging Temperature

The effect of PAG gel temperature during imaging on the N_{CT} -dose response was investigated by obtaining images with PAG gel at 4 °C and comparing these results with the room temperature (~23 °C) results. (Note: all results presented up to this point, except the reproducibility with scanner position, have been room temperature results).

To ensure reproducibility of the 4 °C results, the N_{CT} -dose response for the PAG gel at 4°C was measured on different days (exactly as performed for the room temperature results). The resulting responses are shown in Figure 4.14. As for the room temperature results, the responses are linear up to 8 or 10 Gy and the slope of the response is constant

over different imaging days. A small shift in the N_{CT} - dose response with imaging day is also observed.

The average of the N_{CT} -dose responses obtained on different days, for both gel temperatures of 23 and 4°C, are compared in Figure 4.15. Several key observations are made from this figure. First, there is a shift of approximately +4 H between the 23 and 4 °C results. This shift agrees with the previously observed shift in the N_{CT} of water over the same temperature range (Fallone *et al*, 1982) and is likely due to the increase in the density of water from 997.2965 kg/m³ at 23 °C to 999.972 kg/m³ at 4 °C (CRC Handbook, 1984). The

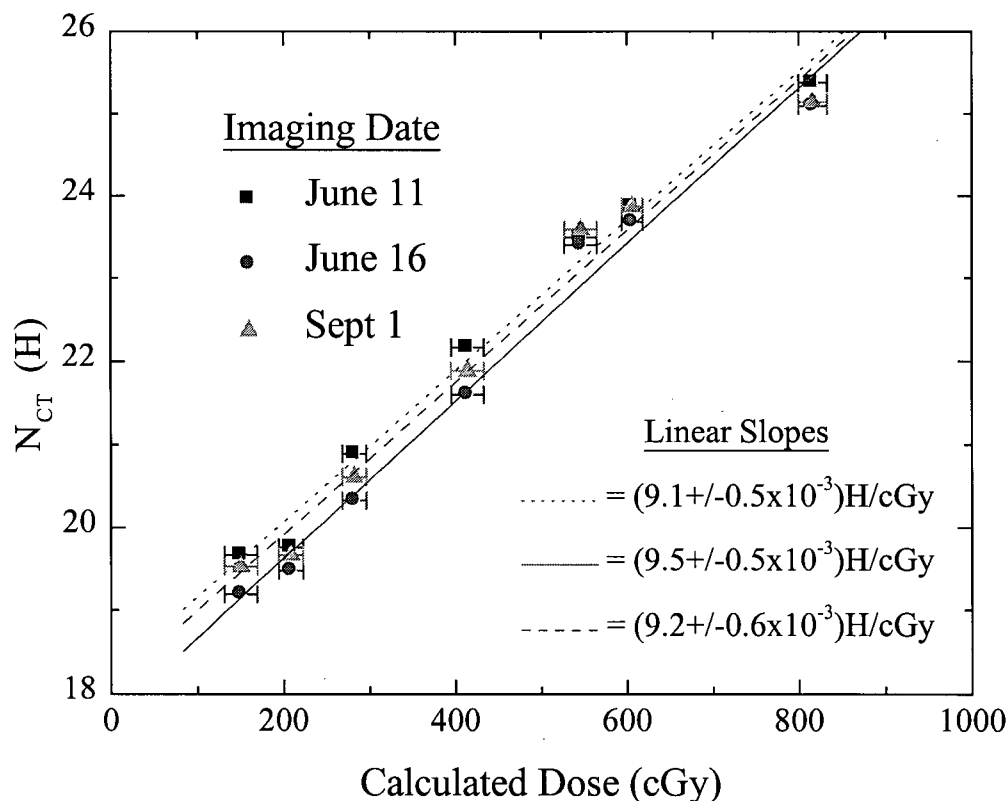


Figure 4.14 N_{CT} - dose response curves obtained over a series of several imaging sessions for our four field PAG gel dosimeter at a temperature of 4°C and the CT imaging protocol was employed (refer to Section 4.1.5). Error bars represent the standard deviation in the average dose measured in regions of interest. Error in N_{CT} , not illustrated, is $\pm 0.5 N_{CT}$ for all data points.

shift in the dose response suggests the need for a baseline calibration measurement during each imaging session when making actual dose measurements, if imaging at an arbitrary temperature.

The N_{CT} -dose sensitivities for the two imaging temperatures are given by the slopes in the following N_{CT} -dose responses for an 8 Gy dose range:

$$N_{CT}(H) = (9.3 \pm 0.5) \times 10^{-3} \text{Dose (cGy)} + \text{constant}; \quad (\text{Gel Temp.} = 4^{\circ}\text{C}) \quad (4.5)$$

$$N_{CT}(H) = (8.5 \pm 0.3) \times 10^{-3} \text{Dose (cGy)} + \text{constant}; \quad (\text{Gel Temp.} = 23^{\circ}\text{C}) \quad (4.6)$$

The magnitude of the change in the sensitivity of the dose response at these temperatures

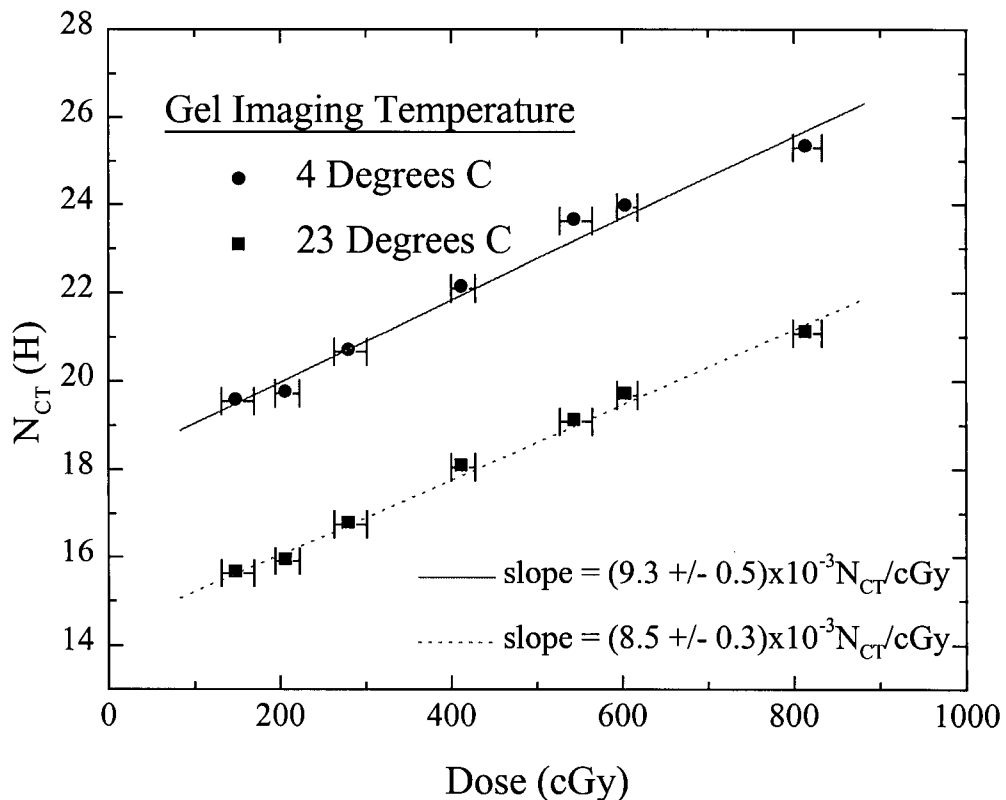


Figure 4.15 Comparison of the average N_{CT} - dose response of our four field PAG gel dosimeter obtained at two different gel temperatures. A shift in N_{CT} and a small change in the slope of the response are observed between the two results. For all images, the CT imaging protocol was employed (refer to Section 4.1.5). Error bars represent the standard deviation in the average dose measured in regions of interest. Error in N_{CT} , not illustrated, is $\pm 0.5 N_{CT}$ for all data points.

only small, $(0.6 \pm 0.2) \times 10^{-3} N_{CT} / \text{cGy}$. Thus, the temperature of the gel during imaging is not critical for determining accurate relative dose measurements. However, given a baseline calibration measurement, in order to obtain accurate relative dose measurements, a response curve must be employed that is not more than approximately 5°C different from the temperature of the gel during imaging. For example, an error on the order of 100cGy would occur in estimating the gel's saturation dose relative to a 0 Gy N_{CT} measurement if a 23°C response curve was used to obtain dose measurements for a gel imaged at 4°C.

Unlike the CT PAG gel dosimetry technique, the MRI PAG gel dosimetry technique is highly sensitive to temperature such that making reproducible dose measurements becomes more of a challenge. For example, a 1°C change in temperature of the gel during MR imaging will produce a dose uncertainty of approximately 50cGy (Audet 1995, Maryanski *et al* 1997).

4.3 Comparison of CT and MRI Techniques

In this section, MRI and CT imaging techniques for performing PAG gel dosimetry are compared. First, doses obtained using both the CT and MRI imaging techniques on the same PAG gel were compared to assess the accuracy of the CT imaging technique (Section 4.3.1). Second, the characteristics of the CT PAG gel dosimetry technique are compared to those of the MRI PAG gel dosimetry technique presented in literature (Section, 4.3.2). Using this comparison, advantages and disadvantages of the two methods are discussed.

4.3.1 Dose Measurement and Localization of High Dose Regions

In order to validate the CT PAG gel dosimetry technique, dose measurements made using the technique were compared to those made using the same gel and the MRI PAG gel dosimetry technique. In particular, the dose profile along the axis of the 6 Gy beam path through the PAG gel (see Figure 4.16) was obtained using the CT and MRI methods and corresponding linear N_{CT} and R_2 - dose responses. The MRI and CT doses agree very well except in the high dose regions (> 10 Gy) of the profiles where neither the linear MRI nor CT dose responses hold. This agreement supports the accuracy and feasibility of CT PAG gel dosimetry despite the low signal to noise ratio and low dose resolution.

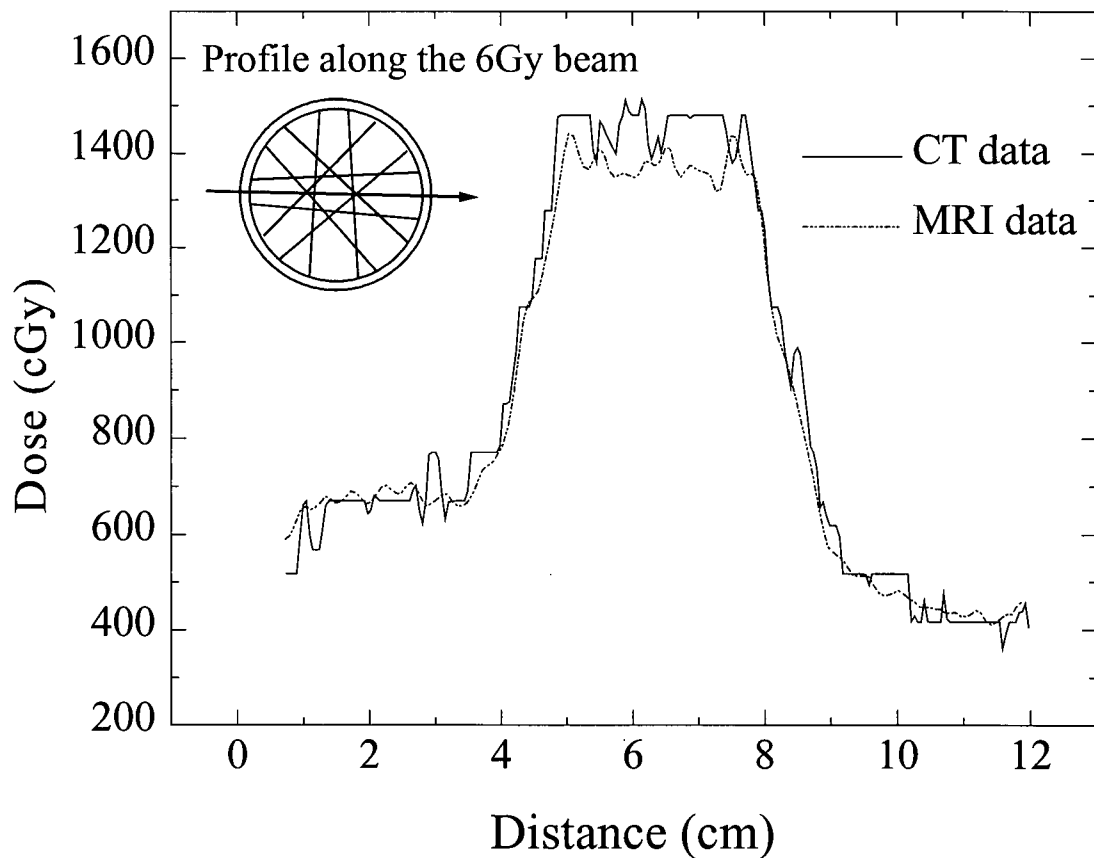


Figure 4.16 Comparison of CT and MR image data illustrating excellent agreement in localization of the high dose region in the four field gel used in this study. The plot shows a 1D profile along the length of the 6 Gy beam from entrance to exit. A 3x3 median filter has been applied to the CT data.

Low dose resolution does not, however, impose limitations on the ability of the CT PAG gel dosimetry technique to localize high dose regions. Figure 4.16 shows that the high dose gradient regions in the MRI and CT dose profiles are well defined spatially and match very well. Hence, the CT-PAG gel dosimetry technique can be used to accurately localize high dose regions provided that a large portion of a PAG gel's dynamic range is exploited. Accurate localization has been observed for a stereotactically irradiated PAG gel using the CT technique (Hilts *et al*, 1999).

4.3.2 Dosimeter Characteristics: Advantages and Disadvantages

Table 4.2 provides a summary of CT PAG gel dosimetry technique characteristics for the imaging protocol summarized in Section 4.1.5. For comparison, corresponding characteristics for the MRI PAG gel dosimetry technique are also listed in Table 4.2 (Olsson, 1998, Audet, 1997, Ibbott, 1997 and Maryanski, 1994).

Table 4.2 Dosimeter characteristics measured for CT PAG gel dosimetry using a GE HiSpeed CT/i[®] CT scanner and the optimum imaging protocol described in Section 4.1. For comparison, MRI PAG gel dosimetry characteristics are cited from literature (Olsson, 1998, Audet, 1997, Ibbott, 1997 and Maryanski, 1994).

Dosimeter Characteristics	CT PAG Gel	MRI PAG Gel
Linear Region	≤ 8 or 10 Gy	≤ 8 or 10 Gy
Degree of Linearity	0.9960	0.988
Dose Response (at 23°C)	$(8.5 \pm 0.3) \times 10^{-3} N_{CT}/cGy$	$2.50 \times 10^{-1} s^{-1}/cGy^*$
Imaging Temperature Effect	3×10^{-5} or 0.34% $N_{CT}/cGy/°C$	8.26×10^{-2} or 33% $s^{-1}/cGy/°C$
Dose Resolution	~ 60 cGy	~ 10 cGy
2D Spatial Resolution	0.5 mm [‡]	~ 1 mm [‡]
Slice Thickness	10 mm	3 mm
Image Time	1 s/slice; 64 s/image	15 min/image [§]

*Dose response for MRI PAG gel dosimetry is a function of magnetic field strength. This response is measured for a 1.5T field.

§ Image time using a single 16-echo CPMG sequence with TR = 3s. Using an alternate technique employing several single echo sequences, image time is around 75 min.

‡ for 25 cm FOV and 256 pixels for MRI and 512 pixels for CT.

Advantages of the CT Imaging Technique

The advantages of using CT to analyse the gels are: 1) the insensitivity of the CT images to imaging temperature; 2) relatively short imaging time; 3) relatively greater spatial resolution in the imaging plane (see Table 4.2); and 4) the accessibility of CT in cancer centres. The effect of imaging temperature on the PAG gel dose response is much smaller when imaging with CT than with MRI. Thus, the time required to equilibrate PAG gel to the temperature of the imaging room when performing MRI is not necessary for CT imaging. Another advantage is that the CT imaging technique requires significantly less imaging time than does the MRI technique. Traditional MRI single echo imaging techniques require approximately 75 min. to obtain an image. The multi-echo CPMG sequence available for this study shortens this imaging time to approximately 15 min and provides high quality images (Audet *et al*, 1997). Regardless, this time is still much more than the 1 min time required to obtain a single averaged CT image. However, this 1 min time may increase if several different slices are required since time will be needed for the x-ray tube to cool down. Since time on diagnostic imaging equipment is extremely valuable, this shorter imaging time required for the CT technique is a great advantage. Another advantage is the increase in spatial resolution in the CT image plane arising from the increased number of pixels chosen to cover a given field of view. For MRI, the lengthy imaging times limit the number of pixels to 256x256, whereas 512x512 pixels are typical for CT. This larger pixel dimension provides the CT PAG gel images with greater spatial resolution in the image plane.

Disadvantages of the CT Imaging Technique

The main disadvantage of a CT imaging technique over an MRI technique is the limited dose resolution (see Table 4.2) which is six times less than the dose resolution for

MRI PAG gel dosimetry. As a result, the CT PAG gel dosimetry technique, although accurate, is not as precise as the MRI technique. This currently limits the use of the CT PAG gel dosimeter technique to: 1) measuring dose distributions that exhibit large changes in dose; and 2) the spatial localization of high dose regions. However, in this preliminary feasibility study the gel formulation has not been optimized for maximizing the sensitivity of density to dose. It is possible that the dose resolution of the CT technique may be improved by using other types of gels.

Another disadvantage of CT imaging PAG gels is the reduced spatial resolution in the slice stacking, or z - direction. As discussed in Section 4.1.2, the loss of resolution in the z-direction in CT PAG gel images results from choosing a 10 mm slice thickness in efforts to improve SNR. The same slice thickness options are available for imaging PAG gel with MRI as with CT, but typically a smaller thickness is chosen for MR images since the SNR is greater. Also, 3D acquisition can be employed with MRI that allows for extraction of slices in any plane though the image volume, increasing resolution and flexibility of 2D image choice. Although in CT imaging, if the phantom were not too large, various imaging planes could be obtained by repositioning the phantom within the scanner bore.

For the remaining dosimetry characteristics listed in Table 4.2, no one imaging technique provides a clear advantage over the other. The range of the linear dose response is the same for both the CT and MRI techniques. Also, for both techniques the response has a high degree of linearity in the 0 – 800 or 1000 cGy range. In summary, the CT PAG gel dosimetry technique eliminates the strong dependence of the dose response on gel imaging temperature as well as the long imaging times, both associated with MRI, however, the CT technique has a much lower dose resolution.

4.4 Quantifying PAG Gel Density

The density of non-irradiated PAG gel (Section 4.4.1) and the density change observed in PAG gel at a high dose (Section 4.4.2) may be quantified. Three independent methods are used to quantify the density of non-irradiated gel (see Section 3.6), and the best of these methods was used to quantify the density change. The density change occurring with dose, for the particular formulation used in this study, is found to be very small thus imposing a fundamental limit on the dose sensitivity of CT gel dosimetry.

4.4.1 Density of Non-irradiated PAG Gel

As previously described, three independent methods were used to determine the density of non-irradiated PAG gel (Section 3.6). The results of these three methods are presented here.

Density Calculated by Mass and Volume Measurements

The PAG gel prepared in a graduated cylinder had a final solidified volume of 55.5 ± 0.5 ml and a mass of 56.29 ± 0.02 g, at 23°C . The resulting physical density for non-irradiated PAG gel was therefore:

$$\rho_{\text{gel}} = 1.018 \pm 0.009 \text{ g/cm}^3 \quad (23^\circ\text{C}) \quad (4.7)$$

Density Calculated from PAG Gel N_{CT} Measurements

Using the method for calculating density from a CT number described in Section 3.6 (Equations 3.1, 3.2 and 3.3), and assuming an effective energy (E_{eff}) of 70.7 ± 1.0 keV for the x-ray tube photon beam, the following physical densities were determined for a non-irradiated PAG gel:

$$\rho_{\text{gel}} = 1.021 \pm 0.001 \text{ g/cm}^3 \text{ at } 23^\circ\text{C} \quad (4.8)$$

$$\rho_{\text{gel}} = 1.028 \pm 0.001 \text{ g/cm}^3 \text{ at } 4^\circ\text{C} \quad (4.9)$$

For the details of this calculation, please see Appendix I. We observe that the 23°C result agrees within error with the PAG gel density measured using mass and volume measurements. Also, there is less uncertainty in this method than in the mass and volume measurement method. However, there may be a systematic error in assuming $E_{\text{eff}} = 70.7 \pm 1.0 \text{ keV}$ (refer to Section 3.6).

Density Determined from an N_{CT} - Density Calibration Curve

N_{CT} values of 15 and 19 H were determined for a non-irradiated PAG gel at imaging temperatures of 23 and 4°C by averaging measurements made from several imaging experiments. Using these average N_{CT} values and the calibration result quoted in Equation 3.5 (Section 3.6), the physical density of the PAG gel at 4 and 23°C was determined. The results are:

$$\rho_{\text{gel}} = 1.023 \pm 0.002 \text{ g/cm}^3 \text{ at } 23^\circ\text{C} \quad (4.10)$$

$$\rho_{\text{gel}} = 1.029 \pm 0.002 \text{ g/cm}^3 \text{ at } 4^\circ\text{C} \quad (4.11)$$

These densities agree very well with the densities determined using the calculation method within error ($1.021 \pm 0.001 \text{ g/cm}^3$ and $1.028 \pm 0.001 \text{ g/cm}^3$ at 4 and 23°C respectively). Average values of $1.022 \pm 0.002 \text{ g/cm}^3$ (23°C) and $1.029 \pm 0.002 \text{ g/cm}^3$ (4°C) are recommended.

4.4.2 Density Change for a High Dose

Given the above three methods for finding PAG gel density, the calibration curve method was determined to be the best method for several reasons. First, although the

density values determined using this method are less precise than those obtained using the calculation method, the approximation of the effective energy of the CT scanner required in the calculation method lends a degree of inaccuracy to the results. Secondly, unlike the effective energy, the calibration curve is produced using the same CT scanner and parameter settings used to provide the N_{CT} measurements for the PAG gel. Thus, this method should be accurate. Finally, the calibration curve method is an accepted technique used in radiation therapy for electron density measurements for treatment planning and it is easy to implement.

For the high dose region in the phantom (~18 Gy), when imaged using the CT imaging protocol (see Section 4.1.5), N_{CT} was measured to be 28 ± 1 H and 31 ± 1 H, at 23 and 4°C respectively. Using Equations 4.10 and 4.11 for the 23 and 4°C measurements, respectively, the physical densities of PAG gel irradiated to 18 Gy were determined to be:

$$\rho_{\text{gel}} = 1.046 \pm 0.002 \text{ g/cm}^3 \text{ at } 23^\circ\text{C} \quad (4.12)$$

$$\rho_{\text{gel}} = 1.050 \pm 0.002 \text{ g/cm}^3 \text{ at } 4^\circ\text{C} \quad (4.13)$$

By comparing these densities to those determined for non-irradiated PAG gel, approximately a 2.2 % post-irradiation density change in the PAG gel is observed for both gel temperatures. This change is very small and implies a fundamental limit to the dose resolution and sensitivity attainable by the CT PAG gel dosimetry technique. Improvement in the dose resolution and sensitivity of a CT gel dosimetry technique will require finding a polymer gel composition that provides greater density changes with absorbed dose.

CHAPTER 5

CONCLUSIONS AND SUMMARY

A novel 3D polymer gel dosimetry technique for measuring 3D dose information with a high spatial accuracy and for verifying conformal radiation techniques is proposed and described. The technique involves analyzing a well known polymer gel dosimeter with x-ray CT instead of MRI or optical CT. Computed Tomography imaging is a fast and accessible means for analyzing irradiated gels. It is accessible since, unlike the other two modalities, it is used for treatment planning purposes in the large majority of radiation therapy clinics or departments. The optimized CT images of an irradiated PAG gel presented in this thesis illustrate the potential of this novel dosimetry technique. The images show dose contrast (Section 4.1) and, combined with reproducible responses of N_{CT} to dose (Section 4.2), can be used to provide actual or relative dose information.

The low dose resolution is currently the limiting factor of the CT PAG gel dosimetry technique, but is by no means the best achievable. It is particular to the PAG gel formulation used in this work and may easily be improved by using gels that show a greater change in density with dose (Section 4.4). A possible improved formulation could result by simply increasing the %T (total amount of monomer) in the PAG gel. The optimization of gel formulation is definitely an area for future studies.

Despite the low dose resolution of the technique, it can accurately localize the high dose volumes (Section 4.3) which typically characterize conformal radiation therapy techniques. Accurate localization has been observed for a stereotactically irradiated PAG gel by Hilts *et al* (1999). In this study, a spherical volume of water was immobilized, CT-

imaged within a fiducially marked box and stereotactically localized and planned. The water was then replaced with PAG gel and the gel irradiated with multiple arcs of a circular field to a maximum dose of 8 Gy. Imaging the irradiated gel with the fiducial box and rerunning the treatment plan on this new set of CT images, allowed for a very simple method of automatically registering the imaged and planned dose distributions. It also allows for a notably convenient way of using the image reconstruction tools of the software to view the correspondence of the two distributions in any plane. Future studies could also involve such applications of the CT gel dosimetry technique to other conformal irradiations. The following summarizes the four major studies in this thesis and their results.

CT Imaging Protocol

A protocol for CT imaging polymer gel was established by choosing image parameter settings that optimized image spatial resolution, contrast and signal to noise ratio. The result of this optimization process included the following CT scanner parameter choices: x-ray tube current = 200 mA, x-ray tube voltage = 120 kV, scan speed = 1 s, reconstruction mode = Detail and slice thickness = 10 mm. Optimizing slice thickness required a compromise between spatial resolution and SNR and, since PAG gel images in general suffer from low SNR, the largest slice thickness of 10 mm was chosen.

The imaging protocol also involved image averaging to increase the SNR in the images. The recommended optimum number of images to average is 64. If a large 3D volume is required then 16 or 32 images per average is recommended. The improvement in SNR revealed ring and beam hardening artifacts that obscured dose information in the images. These artifacts were successfully removed by using a background subtraction

technique. The final images produced using the complete protocol were high quality images that clearly exposed the dose information.

CT Number – Dose Response

After establishing an optimum protocol for CT imaging PAG gel, the CT number - dose response of a PAG gel dosimeter was investigated. Qualitatively, CT number was shown to increase with dose indicating that PAG gel density increases with dose. A potential explanation is the hydrophobicity of polymer. Further investigation revealed that the response was linear over a range of $\sim 200 - 800$ or 1000 cGy, deviating from linearity at higher doses. However, the response does not saturate as drastically as the R_2 - response (Maryanski, 1994, Audet, 1995) and a clear indication of saturation point is difficult. Although, the non-linear response is significant up to at least 18 Gy.

The slope of the linear portion of the response was found to be reproducible for images obtained during a single imaging session and for images obtained during different imaging sessions on different days. This is an encouraging result that implies that a CT PAG gel dosimetry technique can be used to reproducibly measure relative and absolute doses. However, small shifts observed in the absolute CT numbers implies that performing a baseline calibration on the day of imaging would produce actual dose measurements of greater precision.

An investigation of the effect of gel imaging temperature on the dose response illustrated a shift in the response and a small change in dosimeter sensitivity with temperature. There was an average shift of +4 H between the dose responses measured for gel imaging temperatures of 23 and 4 °C. This shift is most likely a result of the density of water increasing from 997.2965 kg/m^3 at 23 °C to 999.972 kg/m^3 at 4 °C (CRC Handbook,

1984). The change in dosimeter sensitivity measured between these temperature results was minimal, $(0.6 \pm 0.2) \times 10^{-3} N_{CT}/\text{cGy}$, and probably within error. The positive benefit of this is that small variations in gel temperature during imaging will not affect dose measurements.

Comparison of CT and MRI Techniques

The dose profiles measured using, and the characteristics of, both the CT and MRI PAG gel imaging techniques were compared in this study. The dose profiles showed excellent agreement, confirming that the CT technique provides accurate dose measurements and localization of high dose regions. The main advantages of using CT over MRI to image PAG gel are: 1) a reduction in the effect of imaging temperature on the dose response; 2) an increase in the spatial resolution in the image plane; 3) substantially shorter imaging time; and 4) the accessibility of CT in cancer centres. The main disadvantage of the CT imaging technique is a dose resolution an order of magnitude less than that of MRI. However, despite the low dose resolution in the CT technique, good agreement is observed between MRI and CT determined doses. Other disadvantages of the CT technique include reduced spatial resolution in the slice stacking direction (compromised for improved SNR), and image acquisition limited to parallel planes through the image volume. The range of the linear dose response and the spatial resolution in the z-direction for both the CT and MRI techniques are comparable.

PAG Gel Density

Several studies were undertaken to provide fundamental information on the density of non-irradiated PAG gel and to quantify the gel's density changes in response to dose. Three independent methods used to determine the density of non-irradiated PAG gel provided consistent results, the average of which is: $\rho_{\text{gel}} = 1.021 \pm 0.004 \text{ g/cm}^3$ at 23°C . Using a

measured calibration curve, the density change observed in the PAG gel in response to ionizing radiation was estimated, for both gel temperatures, to be 2.2 % between the high and zero dose regions of the PAG gel. This minimal change in PAG gel density with dose illustrates a fundamental limit to the dose resolution attainable by a CT PAG gel dosimeter. It is possible this could be improved upon by optimizing the polymer gel composition to provide maximum density change in response to absorbed dose.

REFERENCES

- Attix, FH., Introduction to Radiological Physics and Radiation Dosimetry (John Wiley and Sons, NY, 1986).
- Audet, C., Private communications, (1998).
- Audet, C., Duzenli, C., Schreiner, L.J., Mackay, A., Harrison, R., Mansour, F., Peemoeller, H. "Three dimensional MRI/polymer gel dosimetry: practical considerations", *Medical and Biological Engineering and Computing* **35**, 822 (1997).
- Audet, C., "NMR-dose response studies of the gels used for 3-D radiation dosimetry by magnetic resonance imaging", Ph.D. thesis, McGill University, Montreal, 1995.
- Baldock, C., Rintoul, L., Keevil, SF., Pope, JM., George, GA., "Fourier transform Raman spectroscopy of polyacrylamide gels (PAGs) for radiation dosimetry", *Phys. Med. Biol.* **43**, 3617-3627 (1998).
- Battista, JJ., "Radiotherapy in the Next Millennium" in *Teletherapy: Present and Future*, (American Institute of Physics, NY, 1996).
- Bio-Rad Bulletin *Acrylamide polymerization – a practical approach*, Bio-Rad Bulletin **1156** (1987).
- Boyd, RH., Phillips, PJ., Cambridge Solid State Science Series: The Science of Polymer Molecules (Cambridge University Press, Cambridge, 1993).
- Brooks, RA., "Computational Principles of Transmission CT" in *Medical Physics of CT and Ultrasound: Tissue Imaging and Characterization*, (American Institute of Physics, NY, 1980a).
- Brooks, RA., "Comparative Evaluation of CT Scanner Technology" in *Medical Physics of CT and Ultrasound: Tissue Imaging and Characterization*, (American Institute of Physics, NY, 1980b).
- Curry, TS., Dowdey, JE., Murry, RC., *Christensen's Physics of Diagnostic Radiology* (Lea & Febiger, Malvern, Penn., 1990).
- CRC Handbook of Chemistry and Physics 65th Edition, (CRC Press Inc., Boca Raton, Fl., 1984).

- Dobbs, HJ., Webb, S., "Clinical Applications of X-Ray Computed Tomography in Radiotherapy Planning" in *The Physics of Medical Imaging*, (Institute of Physics Publishing, Philadelphia PA, 1993).
- Fallone, BG., Moran, PR., Podgorsak, EB., "Noninvasive thermometry with a clinical x-ray CT scanner" *Med. Phys.* **9**(5) 715-721 (1982).
- Gordon, R., Herman, GT., "Three-dimensional reconstruction from projections: a review of algorithms", *Int. Rev. of Cytology* **38**(0), 111-51 (1974).
- Gore, JC., Kang, YS., Schulz, RJ., "Measurement of radiation dose distributions by nuclear magnetic resonance (NMR) imaging", *Phys. Med. Biol.* **29**, 1189-1197 (1984a).
- Gore, JC., Kang, YS., Schulz, RJ., "The measurement of radiation dose distributions by magnetic resonance imaging", *Magn. Res. Imaging* **2**, 244 (1984b).
- Gore, JC., Ranade, M., Maryanski, MJ., Schulz, RJ., "Radiation dose distributions in three dimensions from tomographic optical density scanning of polymer gels: I. Development of an optical scanner", *Phys. in Med. & Biol.* **41**(12), 2695-704 (1996).
- Gustavsson, H., Back, SJ., Haraldsson, P., Magnusson, P., Love, P., Olsson, LE., "Treatment planning dose verification using MRI gel dosimetry and a BAREX[®] head and neck phantom", *Proc. "1st Int. Workshop on Rad. Therapy Gel Dosimetry" (Lexington, July 1999)* 210-212.
- Harrison, RM., "External beam treatment planning: Can we deliver what we plan?", *Acta Oncologica* **32**(4), 445-51 (1993).
- Hepworth, S., Morton, E., Doran, S., "Dose distributions beyond air-cavities mapped using polymer gel dosimetry", *Proc. "1st Int. Workshop on Rad. Therapy Gel Dosimetry" (Lexington, July 1999)* 204-206.
- Hilts, M., Duzenli, C., Robar, J., Audet, C., "Polymer gel dosimetry using x-ray computed tomography: Feasibility and potential application to stereotactic radiosurgery", *Proc. "1st Int. Workshop on Rad. Therapy Gel Dosimetry" (Lexington, July 1999)* 204-206.
- HiSpeed CT/i[®] CT Scanner Manual, *GE Medical Systems Rev 4*, (1997).
- Hounsfield, GN., "Computed Medical Imaging", *Science* **210**, 22-28 (1980).
- Hsu, TP., Cohen, C., "Observations on the structure of a polyacrylamide gel from electron micrographs", *Polymer* **32**, 1419-1423 (1984).

- Ibbott, GS., Maryanski, MJ., Eastman, P., Holcomb, SD., Zhang, Y., Avison, RG., Sanders, M., Gore, JC., "Three-dimensional visualization and measurement of conformal dose distributions using magnetic resonance imaging of BANG polymer gel dosimeters", *Int. J. of Rad. Oncology, Biology, Physics* **38**(5), 1097-1103 (1997).
- ICRU Report 50: Prescribing, Recording, and Reporting Photon Beam Therapy*, Bethesda, Maryland, 1993.
- Jayaraman, S., Rozenfeld, M., Lanzl, LH., Chung-Bin, A., "Can the AAPM Task Group 21 protocol lead to optimum ion chamber designs?", *Med. Phys.* **12**(3), 375 (1985).
- Johns, HE., Cunningham, JR., *The Physics of Radiology* (Charles C Thomas Publisher, Springfield, Ill., 1983).
- Karzmark, CJ., "Advances in linear accelerator design for radiotherapy", *Med. Phys.* **11**(2), 105-128 (1984).
- Kaurin, DL., Maryanski, MJ., Duggan, DM., Morton, KC., Coffey, CW., "Use of MRI-based polymer gel dosimetry, pelvic phantom, and virtual simulation to verify setup and calculated three-dimensional dose distribution for a prostate treatment", *Proc. "1st Int. Workshop on Rad. Therapy Gel Dosimetry"* (Lexington, July 1999) 186-189.
- Kelly, RG., Jordan, KJ., Battista, JJ., "Optical CT reconstruction of 3D dose distributions using the ferrous-benzoic-xyleneol (FBX) gel dosimeter", *Med. Phys.* **25**(9), 1741 (1998).
- Kennan, RP., Richardson, KA., Zhong, J., Maryanski, MJ., Gore, JC., "The effects of cross-link density and chemical exchange on magnetization transfer in polyacrylamide gels", *J. of Mag. Res. Series B.* **110**(3), 267-277 (1996).
- Khan, FM., *The Physics of Radiation Therapy* (Williams and Wilkins, Baltimore, 1984).
- Kron, T., Metcalfe, P., Pope, JM., "Investigation of the tissue equivalence of gels used for NMR dosimetry", *Phys. Med. Biol.* **38**, 139-150 (1993).
- Maryanski, MJ., Gore, JC., Kennan, RP., Schulz, RJ., "NMR relaxation enhancement in gels polymerized and cross-linked by ionizing radiation: a new approach to 3-D dosimetry by MRI", *Magn. Res. Imaging* **11**, 253-258 (1993).
- Maryanski, MJ., Schulz, RJ., Ibbott, GS., Gatenby, JC., Xie, J., Horton, D., Gore, JC., "Magnetic resonance imaging of radiation dose distributions using a polymer-gel dosimeter", *Phys. Med. Biol.* **39**, 1437-1455 (1994).

- Maryanski, MJ., Ibbott, GS., Eastman, P., Schulz, RJ., Gore, JC., "Radiation therapy dosimetry using magnetic resonance imaging of polymer gels", *Med. Phys.* **23**(5), 699 (1996a).
- Maryanski, MJ., Zastavker, YZ., Gore, JC., "Radiation dose distributions in three dimensions from tomographic optical density scanning of polymer gels: II. Optical properties of the BANG polymer gel", *Phys. in Med. & Biol.* **41**(12), 2705-17 (1996b).
- Maryanski, MJ., Audet, C., Gore, JC., "Effects of crosslinking and temperature on the dose response of a BANG polymer gel dosimeter", *Phys. Med. Biol.* **42**, 303-311 (1997).
- McCullough, CH., Zink, FE., "CT Numbers and Electron Density" in *Imaging in Radiation Therapy*, (Medical Physics Publishing, WI, 1998).
- McCullough, EC., "CT Imaging Parameters" in *Medical Physics of CT and Ultrasound: Tissue Imaging and Characterization*, (American Institute of Physics, NY, 1980).
- National Cancer Institute of Canada: Canadian Cancer Statistics 1998, Toronto, 1998.
- Niroomand-Rad, A., Blackwell, CR., Coursey, BM., Gall, KP., Galvin, JM., McLaughlin, WL., Meigooni, AS., Nath, R., Rodgers, JE., Soares, CG., "Radiochromic film dosimetry: Recommendations of AAPM Radiation Therapy Committee Task Group 55", *Med. Phys.* **25**(11), 2093-2115 (1998).
- Olsson, LE., "Radiation dosimetry using magnetic resonance imaging", Ph.D. thesis, Lund University, Malmo, Sweden, 1991.
- Olsson, LE., Back, S., Magnusson, P., Haraldsson, P., "3D Dosimetry Using Gels and MRI" in *Imaging in Radiation Therapy*, (Medical Physics Publishing, WI, 1998).
- Pfaender, M., Grebe, G., Budach, V., Wurm, R., "Dosimetry with BANG dosimeters regarding slim shaped parts of lesions for stereotactic radiation with a LINAC and micro-multi-leaf-collimator", *Proc. "1st Int. Workshop on Rad. Therapy Gel Dosimetry"* (Lexington, July 1999) 192-194.
- Pratt, WK., *Digital Image Processing*, (John Wiley and Sons, NY, 1992).
- Ramani, R., Lightstone, A.W., Mason, D.L.D., O'Brien, P.F., "The use of radiochromic film in treatment verification of dynamic stereotactic radiosurgery", *Med. Phys.* **21**, 389-392 (1994).
- Robb, RA., *Three Dimensional Biomedical Imaging: Principles and Practice*, (John Wiley and Sons, NY, 1998).

Schulz, R.J., deGuzman, A.F., Nguyen, D.B., Gore, J.C., "Dose-response curves for Fricke-infused agarose gels as obtained by nuclear magnetic resonance", *Phys. Med. Biol.* **35**, 1611-1622 (1990).

Sprawls, P., "Digital Imaging Concepts and Applications" in *The Expanding Role of Medical Physics in Diagnostic Imaging*, (Advanced Medical Publishing, Madison, 1997).

Swallow, A.J., *Radiation Chemistry: An Introduction*, (John Wiley and Sons, NY, 1973).

Swindell, W., Webb, S., "X-Ray Transmission Computed Tomography" in *The Physics of Medical Imaging*, (Institute of Physics Publishing, Philadelphia PA, 1993).

Task Group 21, Radiation Therapy Committee, AAPM, *Med. Phys.* **10** 741 (1983).

White, D.R., Speller, R.D., "The measurement of effective photon energy and "linearity" in computerized tomography", *Br. J. Radiol.* **53**, 5-11 (1980).

APPENDIX I

PAG gel Density Calculated from Measured N_{CT}

The following provides the details for calculating the density of non-irradiated PAG gel from measurements of N_{CT} made at 4 and 23°C. The method is described more briefly in section 3.6 and the final results are presented in section 4.4.1.

A: General Expression for CT Number

CT number can be expressed as:

$$N_{CT} = 1000 \times \frac{(\rho_{ew}^s - R_\sigma)}{R_\sigma} \quad (1)$$

where ρ_{ew}^s is the electron density of the object being imaged relative to water and R_σ is the ratio of electron cross sections of water and the object being imaged (Kron *et al*, 1993).

B: Electron Densities

In order to employ equation 1, the electron density of the PAG gel must be determined. In general ρ_e , electron density, is given by:

$$\rho_e = \rho \times (\text{number of } e^- \text{ 's/gram}) \quad (2)$$

where ρ is physical density.

The electron densities of water calculated for the two imaging temperatures are presented here:

Imaging Temperature (C)	ρ water (kg/m ³)*	e / g water*	ρ_e water (e / ml)
4	999.972	3.343E+23	3.343E+23
23	997.5385	3.343E+23	3.335E+23

* CRC Handbook, 1984

The electron density of PAG gel is given by:

$$\rho_{e \text{ gel}} = N_A \rho \left[\sum f_i \left(\frac{Z}{A} \right)_i \right] \quad (3)$$

where N_A is Avogadro's constant ($6.023 \times 10^{23} \text{ mol}^{-1}$) and f_i , Z_i and A_i are respectively the fraction by weight, atomic number and atomic mass, of each of the PAG gel components (Kron *et al*, 1993).

The values of Z and A used in calculating the electron densities of constituents of PAG gel, as well as their percent composition in PAG gel, are tabulated below:

PAG gel component	Z	Aw	e / g	% composition
acrylamide	38	71.08	3.22E+23	3
Bis	82	154.17	3.20E+23	3
Gelatin	52.3	97.8	3.22E+23	5
Water			* 3.343E+23	89

* from the CRC Handbook instead of calculated

Using the values presented above, the number of electrons per gram for the PAG gel is determined to be $3.326 \times 10^{23} \text{ e}^-/\text{g}$.

Following equation 2, the electron density of PAG gel is given by:

$$\rho_{e \text{ gel}} = 3.326 \times 10^{23} \rho_{\text{gel}} \quad (4)$$

C: The Ratio of Electron Densities of Water and PAG Gel

To employ equation 1, the relative electron density of the object being image compared to water, ρ_{ew}^s , must be calculated. It is given by:

$$\rho_{ew}^s = \frac{\rho_{e \text{ gel}}}{\rho_{ew}} \quad (5)$$

Using our results from section B, above, values for ρ_{ew}^s were calculated for PAG gel imaging temperatures of 4 and 23°C. These results are tabulated here:

Imaging Temperature (C)	Relative ρ_e
4	0.9949 ρ_{gel}
23	0.9973 ρ_{gel}

D: Ratio of the Electronic Cross Sections of Water and PAG Gel:

The final value required in order to employ equation 1 is R_{σ} , the ratio of electronic cross sections. This ratio is given by:

$$R_{\sigma} = \left[\sum f_i \left(\frac{\mu}{\rho} \right)_i \left(\frac{A}{Z} \right)_i \right]_{sample}^{water} \quad (6)$$

where μ/ρ , Z , A and f_i are respectively the mass attenuation coefficient, atomic number, atomic mass and fraction by weight of element i (Kron *et al*, 1993).

As discussed in section 2.1.1, attenuation coefficients depend on energy, and as a result the beam energy of the CT scanner must be known. Since the output from an x-ray tube is a polyenergetic beam, it must be approximated by a monoenergetic beam, or an “effective” beam energy. As stated in the literature, for a 120 kV tube voltage setting, the effective energy of a typical diagnostic CT x-ray tube is 70.7 ± 1.0 keV (White, et al, 1980). This value is employed here as the effective energy of the x-ray tube of the GE HiSpeed CT/i[®] scanner, however, it is only an approximate value since it is expected that effective energy will vary slightly with x-ray tube model and age. Employing this effective energy, the following table lists the values that were used to calculate the electron cross section for water and for PAG gel:

Element	A / Z	μ / ρ *	fw (water)	fg (gelatin)	fa (acrylamide)	fb (Bis)
H	1.00797	0.3169	0.112	0.071	0.071	0.065
O	1.9999	0.1773	0.888	0.363	0.225	0.208
C	2.0018	0.1671	----	0.422	0.507	0.545
N	2.0010	0.1715	----	0.143	0.197	0.182

* for 70.7 ± 1.0 keV, the effective energy for a 120 kV tube voltage setting (Johns and Cunningham).

Employing these values, the resulting ratio of electron cross sections shown here:

σ water	σ BANG gel	R_{σ}
0.3511	0.349945	1.0033 +/- 0.0001 d

^d given a +/- 1 keV uncertainty in effective x-ray tube energy

E: Resulting Calculations of the Density of PAG Gel

Using equation 1 and the average CT numbers measured for blank PAG gel at 4 and 23°C, PAG gel densities at these two temperatures are calculated. The results, shown in table form below, are also presented in section 4.4.1:

Imaging Temperature (C)	N_{CT} non-irradiated BANG gel	ρ non-irradiated BANG gel (g/cm ³)
4	19 +/- 1	1.028 +/- 0.001
23	15 +/- 1	1.021 +/- 0.001